Earth Surf. Dynam. Discuss., doi:10.5194/esurf-2015-52, 2016
Manuscript under review for journal Earth Surf. Dynam.
Published: 19 January 2016

Earth Surface Dynamics Discussions

Gravel threshold of motion: A state function of sediment transport disequilibrium?

Joel P. L. Johnson

Department of Geological Sciences, The University of Texas at Austin

Correspondence to: joelj@jsg.utexas.edu

Abstract

In most sediment transport models, a threshold variable dictates the shear stress at which non-negligible bedload transport begins. Previous work has demonstrated that nondimensional transport thresholds (τ_c^*) vary with many factors related not only to grain size and shape, but also with characteristics of the flow and surrounding grains. Both a conceptual model and flume experiments suggest that τ_c^* should evolve as a function of local entrainment and deposition. Net entrainment preferentially removes more mobile particles while leaving behind more stable grains, gradually increasing τ_c^* and reducing transport rates. Net deposition tends to fill in topographic lows, progressively leading to less stable distributions of surface grains, decreasing τ_c^* and increasing transport rates. A new model is proposed for the temporal evolution of τ_c^* as a power-law function of net erosion or deposition, which shares some similarities with the Exner equation. Model parameters are calibrated based on flume experiments that explore transport disequilibrium. The τ_c^*-evolution equation is then incorporated into a simple morphodynamic model. The evolution of τ_c^* acts as negative feedbacks on morphologic change, while also allowing reaches to equilibrate to sediment supply at different slopes. Finally, τ_c^* is interpreted to be an important but nonunique state variable for channel morphology, in a manner consistent with the role that state variables such as temperature play in describing the evolution of thermodynamic systems.

Earth Surf. Dynam. Discuss., doi:10.5194/esurf-2015-52, 2016
Manuscript under review for journal Earth Surf. Dynam.
Published: 19 January 2016

Earth Surface Dynamics Discussions

1 Motivation

Despite over a century of quantitative study (Gilbert, 1914), it often remains challenging to predict coarse bedload transport rates to much better than an order of magnitude because of the complexity of grain interactions with the flow and the surrounding grains. Predictive models for complex systems often derive utility from their simplicity, as is the case with the widely used Meyer-Peter and Müller (1948) transport equation, as modified by Wong and Parker (2006):

$$q_s^* = 3.97\left(\tau^* - \tau_c^*\right)^{1.5} \qquad \text{for} \qquad \tau^* \geq \tau_c^* \tag{1}$$

where q_s^* is a nondimensional sediment transport rate per unit width, τ^* is a nondimensional shear stress imparted by the fluid on the channel bed (a Shields stress), and τ_c^* is the nondimensional threshold stress at which grains begin to move (a critical Shields stress). Variables are nondimensionalized as followed:

$$q_s^* = \frac{q_s}{D\sqrt{\left(\frac{\rho_s}{\rho} - 1\right)gD}} \tag{2}$$

$$\tau^* = \frac{\tau}{(\rho_s - \rho)gD} \tag{3}$$

where q_s is volume sediment transport rate per unit width (m^2/s), D is grain diameter (m), ρ_s is sediment density (m^3/kg), ρ is water density (m^3/kg), g is gravitational acceleration (m/s^2), and τ is shear stress (Pa). In principle, these nondimensionalizations should account for differences in grain size, fluid and sediment density and gravity, allowing meaningful comparisons of transport and stress across different conditions. For a given grain diameter (and ~constant ρ_s, ρ and g assumed for terrestrial landscapes), the simplicity of Eq. (1) is that it predicts transport rate using just two variables, τ^* (a function of flow strength) and τ_c^* (a function of many variables). In practice, τ_c^* is often back-calculated from a particular sediment transport model. For example, the Meyer-Peter and Muller (1948) τ^* and q_s^* give best-fit τ_c^*=0.0495 for Eq. (1) (Wong and Parker, 2006). In practice, τ_c^* can essentially be an empirical fitting parameter for a given transport model (e.g., Wong and Parker, 2006; Buffington and Montgomery, 1997).

Earth Surf. Dynam. Discuss., doi:10.5194/esurf-2015-52, 2016
Manuscript under review for journal Earth Surf. Dynam.
Published: 19 January 2016

Thresholds of motion for gravel often span an order of magnitude or more (Fig. 1; see caption for data sources). Variability in τ_c^* greatly influences bedload flux predictions in mountain rivers because transport occurs close to thresholds conditions, even during large floods (Phillips et al., 2013; Parker et al., 1982; Parker and Klingeman, 1982). Previous work demonstrates a great many factors that can collectively cause τ_c^* scatter; for example, slope can empirically explain 34% of the variability shown in Fig. 1 data (e.g., Buffington and Montgomery, 1997; Kirchner et al., 1990; Lamb et al., 2008). Although interrelated, τ_c^* influences can generally be classified as grain controls, "bed state" controls, and flow controls. In addition to diameter and density, grain controls include shape and angularity (e.g., Prancevic and Lamb, 2015; Gogus and Defne, 2005). Bed surface controls include the grain size distribution (GSD) of the surrounding bed, the degree of overlap and interlocking among grains, the protrusion of grains into the flow, the degree of coarse grain clustering, the bed roughness, and the reach slope (e.g., Parker, 1990; Wilcock and Crowe, 2003; Sanguinito and Johnson, 2012; Buscombe and Conley, 2012; Mao, 2012; Kirchner et al., 1990; Strom and Papanicolaou, 2009; Marquis and Roy, 2012; Powell and Ashworth, 1995; Richards and Clifford, 1991). Flow characteristics influencing τ_c^* include particle Reynolds number, flow depth relative to grain size, the intensity of turbulence, the history of prior flow both above and below transport thresholds, and the partitioning of stress into form drag and skin friction (e.g., Shvidchenko and Pender, 2000; Ockelford and Haynes, 2013; Schneider et al., 2015a). However, most flow-dependent controls are not independent of the bed surface controls. For example, flow depths, turbulence and form drag depend on slope and bed roughness, while the stress history influences τ_c^* by changing grain interlocking and surface roughness.

In addition, recent work suggests that the amount of sediment supplied from upstream affects τ_c^*, with higher rates of upstream supply corresponding to more mobile sediment and lower τ_c^* (Recking, 2012; Bunte et al., 2013). Sensitivity of τ_c^* to sediment flux is not obviously classifiable as either a flow or a bed state control. The idea that transport rate influences τ_c^* is intriguing because, by definition, τ_c^* influences transport rate (Eq. 1). This feedback is the focus of the present analysis. A constant τ_c^* is commonly assumed for gravel transport calculations, perhaps for several reasons. First, the traditional Shields diagram indicates that τ_c^* is rather insensitive to particle Reynolds number once flow becomes

Earth Surf. Dynam. Discuss., doi:10.5194/esurf-2015-52, 2016
Manuscript under review for journal Earth Surf. Dynam.
Published: 19 January 2016

hydraulically rough around grains (Buffington, 1999). Second, a belief that τ_c^* is fundamentally a material property of a grain rather than a bed state control also remains somewhat ingrained. Third, because the best estimate of a given variable is usually its average, there is a tendency to attribute variability to measurement noise and uncertainty, even when that variability may be real, its causes understandable, and its influence potentially important to system dynamics (Jerolmack, 2011; Buffington and Montgomery, 1997).

Feedback between channel morphology and bedload transport defines morphodynamics. The Exner equation of sediment mass balance quantifies how transport changes correspond to topographic changes (Paola and Voller, 2005):

$$\frac{\partial z}{\partial t} = -\left(\frac{1}{1-\lambda_p}\right)\frac{\partial q_s}{\partial x} \quad (4)$$

where z is bed elevation (vertical position) x is horizontal position, t is time, and λ_p is bed porosity. Sediment flux and bed elevation are functions of both position and time. In this morphodynamic equation (presented for simplicity without an uplift or subsidence term), topographic equilibrium ($\partial z/\partial t = 0$) is attained when the sediment flux into a reach equals the sediment flux out ($\partial q_s/\partial x = 0$). Channel morphology has long been recognized to influence sediment transport. Of particular relevance to the present work, Stark and Stark (2001) proposed an insightful landscape evolution model with a variable called *channelization* that is defined as representing "the ease with which sediment can flux through a channel reach" (Stark and Stark, 2001). Conceptually, channelization characterizes how changes in reach morphology influence local transport rate. However, channelization is an abstract unitless number that does not correspond physically to any measureable aspects of morphology. A fundamental feedback is imposed in the model: channelization evolves through time as a function of both sediment flux and of itself, resulting in a differential equation. The combination of local slope and channelization tend to asymptote towards values such that $\partial q_s/\partial x = 0$, i.e. transport equilibrium. For a given upstream sediment supply rate, a modeled reach can evolve to equilibrium at different slopes (for different corresponding values of channelization) because both slope and channelization affect transport rate.

Interestingly, the above definition of channelization could also be applied to τ_c^*. Because of its control on transport rates, changes in τ_c^* should influence channel

Earth Surf. Dynam. Discuss., doi:10.5194/esurf-2015-52, 2016
Manuscript under review for journal Earth Surf. Dynam.
Published: 19 January 2016

morphodynamics, both over human timescales (e.g., in response to natural and anthropogenic perturbations such as landslides, floods, post-wildfire erosion, land use, changing climate) and longer timescales (landscape evolution). The overall goal of the present work is to elucidate possible feedbacks among thresholds of motion, changes in transport rate, and the morphological evolution of channels. A motivating hypothesis is that variability in gravel τ_c^* is both physically meaningful and reflects changes in τ_c^* as a predictable function of sediment flux. Another hypothesis is that the implicit effects of multiple processes on τ_c^* can collectively be accounted for in terms of sediment flux dependence. Because changes in alluvial channel morphology are strongly coupled with sediment flux (Eq. 4), I also hypothesize that the evolution of τ_c^* can implicitly model effects of evolving channel morphology.

The paper is organized as follows. First, a conceptual model for why τ_c^* should depend on sediment flux is presented, followed by equations. Next, flume experiments on mixed grain size transport are used to empirically calibrate model parameters. The experimental data are consistent with the Wilcock and Crowe (2003) hiding function that predicts transport rates for grain size mixtures. A simple morphodynamic model is then used to evaluate how evolving τ_c^* influences timescales of channel profile evolution. Finally, in the discussion section τ_c^* is argued to be one of many "state variables" that can describe how channels evolve in response to external forcing and internal feedbacks. Comparisons are made to state variables in thermodynamics.

2 Models and Methods

2.1 Conceptual framework for τ_c^* evolution

For bed surface grains of a given size class, τ_c^* actually represents the stress at which only the most mobile of those grains become entrained. Individual grains will each have a different threshold based on the pocket geometry and near-bed flow velocity at its particular location, resulting in τ_c^* probability distributions when considering all similarly sized grains (Kirchner et al., 1990; Buffington et al., 1992). Gravel flux increases with discharge primarily

Earth Surf. Dynam. Discuss., doi:10.5194/esurf-2015-52, 2016
Manuscript under review for journal Earth Surf. Dynam.
Published: 19 January 2016

because thresholds are gradually exceeded for increasing proportions of surface grains of a given size. When the sediment flux entering a reach— $q_{\sin}$ —is balanced by the flux exiting— q_{sout} —it is assumed that the τ_c^* probability distribution does not change over time, and that τ_c^* remains constant.

In the case of a channel reach undergoing net erosion ($q_{sout} > q_{\sin}$, so $\partial q_s / \partial x > 0$), the most mobile grains would preferentially be entrained first. Progressive erosion will entrain grains from increasingly more stable positions on the bed, gradually increasing τ_c^*. Conversely, during net deposition, grains will tend to preferentially deposit in more stable bed positions such as local topographic lows. Continued deposition would lead to grains being deposited in progressively less stable positions, gradually decreasing τ_c^*. These changes describe negative transport feedbacks: net erosion progressively reduces rates of erosion by making grains harder to entrain, while net deposition progressively makes grains more mobile and less likely to be deposited.

The amount by which τ_c^* changes should also depend on the current state of the bed surface. If bed surface grains are already loosely packed and highly mobile, additional deposition would cause little additional decrease in τ_c^*. On the other hand, initial deposition onto a stable bed would likely cause bigger reductions in τ_c^* than subsequent deposition. Thus, the change in τ_c^* should also be a function of τ_c^*.

Two additional points need to be made. First, natural sediment is a mixture of sizes. It is common to assume that a single representative grain size, such as the median (D_{50}), adequately describes transport of the whole mixture. Second, "thresholds" can represent different things in different models. In Eq. (1), $\tau^* = \tau_c^*$ represents a modeled transport rate of zero. In other models designed to predict measurable transport rates at very low shear stresses, a non-threshold "reference" stress is instead defined as the Shields stress at which q_s^* has a very low but specific nonzero value (Parker, 1990; Wilcock and Crowe, 2003). For many applications the practical difference between threshold and reference stresses are negligible (Buffington and Montgomery, 1997), and in the present work they are largely used interchangeably.

Earth Surf. Dynam. Discuss., doi:10.5194/esurf-2015-52, 2016
Manuscript under review for journal Earth Surf. Dynam.
Published: 19 January 2016

2.2 τ_c^*-evolution model equations

Because longitudinal coordinate *x* increases downstream, net deposition in a reach is indicated by $\partial q_s/\partial x < 0$ and local erosion by $\partial q_s/\partial x > 0$. The following relations are proposed:

$$\frac{\partial \tau_c^*}{\partial t} = \begin{cases} kB\left(\left|\frac{\partial q_s}{\partial x}\right|\right)^{\kappa_{ent}} & if \quad \partial q_s/\partial x > 0 \\ -k(1-B)\left(\left|\frac{\partial q_s}{\partial x}\right|\right)^{\kappa_{dep}} & if \quad \partial q_s/\partial x < 0 \end{cases} \tag{5}$$

$$B = \frac{\tau_{c\max}^* - \tau_c^*}{\tau_{c\max}^* - \tau_{c\min}^*} \tag{6}$$

where κ_{ent} and κ_{dep} are dimensionless exponents corresponding to entrainment and deposition, respectively, and *k* is a scaling factor. These three parameters will be empirically fit to experiments. $\tau_{c\min}^*$ and $\tau_{c\max}^*$ represent bounds on how low or high τ_c^* can plausibly evolve (assumed to be 0.02 and 0.35 respectively). Eq. (5) predicts that τ_c^* incrementally decreases when net deposition occurs, and incrementally increases during net erosion in a reach. "Feedback factor" *B* makes Eq. (5) a differential equation; it scales the incremental change in τ_c^* such that deposition on an already "loose" bed (τ_c^* close to $\tau_{c\min}^*$) would be minimally decrease τ_c^*, but erosion would cause a larger incremental τ_c^* increase. Conversely, if τ_c^* were already high (close to $\tau_{c\max}^*$), then erosion would cause a much smaller τ_c^* change than deposition. Finally, we note that representing $\partial \tau_c^*/\partial t$ as a function of $\partial q_s/\partial x$ is broadly analogous in form to Exner (Eq. 4).

A limitation of Eq. (5) is that, for dimensionally consistency, the units of *k* vary with κ_{ent} and κ_{dep}. An improved equation replaces spatial changes in flux with spatial changes in the thickness of deposited or eroded sediment:

$$\frac{\partial \tau_c^*}{\partial t} = \begin{cases} kA_r B\left(\left|\frac{\partial \theta_s}{\partial x}\right|\right)^{\kappa_{ent}} & if \quad \partial q_s/\partial x > 0 \\ -kA_r(1-B)\left(\left|\frac{\partial \theta_s}{\partial x}\right|\right)^{\kappa_{dep}} & if \quad \partial q_s/\partial x < 0 \end{cases} \tag{7}$$

Earth Surf. Dynam. Discuss., doi:10.5194/esurf-2015-52, 2016
Manuscript under review for journal Earth Surf. Dynam.
Published: 19 January 2016

189 A_r is an optional dimensionless armoring parameter, described further below. θ_s is the
190 thickness of sediment deposited or eroded at a given location; it has dimensions of length.
191 $\partial\theta_s/\partial x$ is a dimensionless ratio representing spatial changes in erosion and deposition. In this
192 case, k has dimensions $1/t$ and scales how quickly τ_c^* evolves. θ_s can calculated by
193 integrating Eq. (4) over time interval t_1 to t_2:

194 $$\theta_s(t_2,x) = z(t_2,x) - z(t_1,x) = \frac{1}{1-\lambda_p}\int_{t_1}^{t_2}\frac{\partial q_s(t,x)}{\partial x}dt \qquad (8)$$

195 (recall that $\int_a^b(\partial f(s,t)/\partial t)dt = f(s,b) - f(s,a)$ for a generic function f). Using discrete flume
196 data, θ_s is calculated over a measurement interval Δt as $(1-\lambda_p)^{-1}(\overline{q_{sout}} - \overline{q_{\sin}})\Delta t/\Delta x$, where
197 Δx is the length of the flume and the sediment flux terms are averaged over Δt.

198 While A_r is set to 1 for many calculations below, the parameter is included in order to
199 explore whether other metrics of relative surface grain size variability or bed roughness
200 improve predictions. For example, the rate at which τ_c^* changes might depend on grain size
201 relative to bed surface roughness (σ), i.e. $A_r = D_{50}/\sigma$. Setting $A_r = D_{50}/\sigma$ suggests that,
202 relative to topographic lows and highs, large range cause bigger τ_c^* changes than small grains.

203 ### 2.3 Experimental design

204 The flume experiments used to calibrate k, κ_{ent} and κ_{dep} explore how fine gravel
205 pulses influence the morphodynamics of step-pool like channels. Johnson et al. (2015)
206 provide details of the experimental conditions and how they scale to natural conditions, and
207 so the summary here is brief. Four experiments were conducted in a small flume 4 long and
208 10 cm wide. Experiments 1 and 4 were done at 8% initial slope, and 2 and 3 at 12% initial
209 slope. Water discharge was held constant throughout to better isolate the influence of
210 sediment supply changes on transport. Sediment transported out of the flume over different
211 time intervals was caught in a downstream basket, sieved and weighed. Sediment was painted
212 different colors based on five size classes with median diameters 2.4, 4.5, 8.0, 15.4, and 27.2
213 mm. Surface GSDs were measured using image analysis of colored bed surface grains during
214 the experiments. Bed topography was measured using a triangulating laser, and bed roughness
215 (σ) was calculated from longitudinal topographic swaths as the standard deviation of

Earth Surf. Dynam. Discuss., doi:10.5194/esurf-2015-52, 2016
Manuscript under review for journal Earth Surf. Dynam.
Published: 19 January 2016

detrended bed elevations. Water surface elevations were measured using an ultrasonic distance sensor, and water depths were calculated by subtracting bed elevations. Total shear stress (τ) was calculated assuming steady uniform flow when spatially averaged over the flume:

$$\tau = \rho g h S \quad (9)$$

where h is water depth corrected for sidewall effects following the method of Wong and Parker (2006), and S is water surface slope.

The experiments started with mixed-size sediment screeded flat. Initially, all surface sizes were observed to be mobile (and therefore above thresholds of grain motion). At the beginning no sediment was fed into the upstream end ($q_{\sin}$ =0), and the bed responded by coarsening, roughening and some net erosion. The bed gradually stabilized and transport rates dropped to be very low. After this initial bed stabilization, a step-function pulse of the finest gravel size (D_{50}=2.4 mm) was fed into the flume at 1000 g/min, representing an idealization of a landslide, debris flow, post-wildfire erosion, anthropogenic gravel augmentation, or similar process that would suddenly supply a prolonged pulse of sediment finer than the existing bed surface. Initially some deposition occurred on the bed, but the channel adjusted rapidly, by both entraining coarser bed surface grains and transporting most of the finer supplied gravel, so that the outlet transport rate (q_{sout}) approximately matched $q_{\sin}$. After the sediment supply pulse $q_{\sin}$ was again dropped to zero, and the bed gradually restabilized, asymptotically approaching though not quite attaining equilibrium transport ($q_{sout} \approx 0$) during the remainder of each experiment.

2.4 The Wilcock and Crowe (2003) transport model

As described above, τ_c^* is often calculated by fitting a sediment transport model to data. Experimental shear stresses and GSDs provide all of the variables needed to evaluate the "Surface-based Transport Model for Mixed-Size Sediment" of Wilcock and Crowe (2003), abbreviated as W&CM. A goal is to evaluate how well the W&CM can predict transport in the present experiments, which used steeper reach slopes and lower water depths relative to GSDs compared to experiments of Wilcock and Crowe (2003). In addition, disequilibrium transport was intentionally quantified during supply perturbations that caused net deposition

Earth Surf. Dynam. Discuss., doi:10.5194/esurf-2015-52, 2016
Manuscript under review for journal Earth Surf. Dynam.
Published: 19 January 2016

or erosion. In contrast, the experiments Wilcock and Crowe (2003) used to calibrate their model intentionally reflected steady-state transport.

A central variable in the W&CM is τ_{rs50}, the reference stress for the median *surface* grain size (D_{s50}). The nondimensional equivalent is τ^*_{rs50} (Eq. 3). Rather than being an actual threshold (i.e., τ^*_c), τ^*_{rs50} corresponds to a very low transport rate of W_i^*=0.002. W_i^* is a nondimensional bedload transport rate for grain size class *i*,

$$W_i^* = \left(\frac{\rho_s}{\rho} - 1\right)\frac{g q_{bi}}{F_i u_\tau^3} \tag{10}$$

where q_{bi} is the volumetric transport rate per unit channel width of grains of size *i*, F_i is the fraction of size *i* on the bed surface, and u_τ is shear velocity ($u_\tau = \sqrt{\tau/\rho}$). Wilcock and Crowe (2003) presented an empirical relationship between transport and shear stress:

$$W_i^* = \begin{cases} 0.002\left(\dfrac{\tau}{\tau_{ri}}\right)^{7.5} & for \quad \tau/\tau_{ri} < 1.35 \\ 14\left(1 - \dfrac{0.894}{\left(\dfrac{\tau}{\tau_{ri}}\right)^{0.5}}\right)^{4.5} & for \quad \tau/\tau_{ri} \geq 1.35 \end{cases} \tag{11}$$

where τ_{ri} is a dimensional reference stress for size class *i*, with dimensionless equivalent τ^*_{ri} (Eq. 3). A "hiding function" determines how nondimensional reference stresses vary with grain size:

$$\frac{\tau^*_{ri}}{\tau^*_{rs50}} = \left(\frac{D_i}{D_{s50}}\right)^{b-1} \tag{12}$$

Hiding function exponent *b* is calculated as

$$b = \frac{0.67}{1 + e^{(1.5 - D_i/D_{s50})}} \tag{13}$$

Note that the W&CM *b* relation was slightly modified by replacing D_{sm} (the geometric mean surface diameter) with D_{s50}, to more simply use just one measure of the central tendency of

Earth Surf. Dynam. Discuss., doi:10.5194/esurf-2015-52, 2016
Manuscript under review for journal Earth Surf. Dynam.
Published: 19 January 2016

the surface GSD. The additional dependence of τ^*_{rs50} on surface sand fractions in this model will be addressed below.

3 Results

3.1 Experimental data and best-fit τ^*_{rs50}, hiding functions

Transport rates, surface grain size, and reach slopes evolved during the experiments as the flume beds initially stabilized, then responded to the pulse of sediment supply, and finally restabilized (Fig. 2). Johnson et al. (2015) explained in detail how the addition of gravels finer than the stabilized bed surface ultimately caused further surface coarsening. Relevant to the present analysis, transport rates in and out of the flume are not always balanced (Fig. 2a), although transport evolves towards this equilibrium condition.

The experimental data are used to determine W_i^* (Eq. 10) and then τ^*_{ri} for each of the five size classes (Eq. 11). Best-fit τ^*_{rs50} is then calculated in two ways. In the first approach, *b* is simply calculated using Eq. (13). Nonlinear multiple regression (in Matlab) is then used for best-fit parameter estimation of τ^*_{rs50} and 95% confidence intervals for each experimental time step (Fig. 3, "W&C fit"). A key point to emphasize is that experimental grain size changes do not explain the temporal evolution of best-fit τ^*_{rs50}, because in this analysis the W&CM should already account for grain size changes in terms of D_i/D_{s50} (Eq. 12, 13). Also note that a form drag correction was not done; transport was calculated in terms of total stress (Eq. 9; section 5.5).

While hiding function exponent *b* varies with relative grain size in the W&CM (Eq. 13), other proposed hiding functions have usually found (or assumed) that a single *b* value applies to different grain sizes, at least for a given set of flow and surface conditions (Parker, 1990; Buscombe and Conley, 2012). The second approach explores whether τ^*_{rs50} estimates are sensitive to details of the hiding function exponent. Rather than using Eq. (13), *b* is empirically fit as single values (for all grain size classes), but with different fits to *b* for each separate time step. Nonlinear multiple regression was used to estimate both *b* and τ^*_{rs50} in Eq. (12) (Fig. 3). Although the 95% confidence intervals tend to be larger because both *b* and

Earth Surf. Dynam. Discuss., doi:10.5194/esurf-2015-52, 2016
Manuscript under review for journal Earth Surf. Dynam.
Published: 19 January 2016

292 τ^*_{rs50} were estimated rather than just τ^*_{rs50}, the temporal evolution of experimental τ^*_{rs50} is
293 comparable for the two different approaches (Fig. 3).

294 Interestingly, these experiments are consistent with the particular grain size-dependent
295 *b* function proposed by Wilcock and Crowe (2003) (Eq. 13). Fig. 4 shows data points
296 determined using the *b* and τ^*_{rs50} regressions, *not* using Eq. (13). In spite of substantial scatter
297 there is a slope break which corresponds to a change in *b* for surface grains smaller and larger
298 than the median.

299 **3.2 Calibration of τ^*_c-evolution model parameters**

300 Fig. 5 compares the experiment and W&CM-based calculation of τ^*_{rs50} to several
301 predictions of these trends. First, a sand fraction dependence is explored. A unique aspect of
302 the W&CM not described above is that changes in surface sand fraction could cause temporal
303 evolution of τ^*_{rs50}. In particular, Wilcock and Crowe (2003) proposed that τ^*_{rs50} varied
304 systematically from 0.036 with no surface sand to 0.021 with abundant surface sand:

305 $$\tau^*_{rs50} = c_1 + c_2 e^{-c_3 F_s} \quad (14)$$

306 where F_s is the fraction of sand on the bed surface, and constants c_1, c_2 and c_3 were
307 empirically found by them to be 0.021, 0.015 and 20 respectively (for simplicity, the
308 geometric mean reference stress was again replaced in their original equation with τ^*_{rs50}).
309 Subsequent work has shown that thresholds of motion can similarly be reduced by grains
310 substantially smaller than the bed surface but larger than sand (Venditti et al., 2010; Sklar et
311 al., 2009; Johnson et al., 2015), suggesting that the "sand fraction" effect could also be
312 modeled for grains larger than 2 mm.

313 In the present experiments, the surface fraction of actual sand (<2 mm) was very
314 small. However, because grains larger than sand but smaller than the average bed surface
315 may also enhance mobility, we evaluate whether Eq. (14) can explain the experimentally-
316 constrained variations in τ^*_{rs50}. Using the surface fraction of grains < 2.8 mm (representing the
317 smallest grain size class in the experiments), a nonlinear multiple regression of Eq. (14) to all
318 four experiments together yielded a poor although statistically significant fit to the data

Earth Surf. Dynam. Discuss., doi:10.5194/esurf-2015-52, 2016
Manuscript under review for journal Earth Surf. Dynam.
Published: 19 January 2016

(R^2=0.13; p=3x10^{-5}; c_1=0.097±0.04, c_2=0.103±0.11, and c_3=5.6±11), confirming that surface grain size changes alone cannot explain observed τ^*_{rs50} patterns (Fig. 5, "Sand fraction").

My proposed τ^*_c-evolution models that instead depend on transport disequilibrium provide much better fits to experimentally-constrained τ^*_{rs50}. Fig. 5 shows model fits using Eq. (7) with A_r=1, both for a single set of model parameters that provide the best fit to all four experiments together ("collective best fit", k=0.17, κ_{dep}=0.20, κ_{ent}=0.40), and also best fits for each of the four experiments separately. The best-fit overall model has R^2=0.69, suggesting statistically that effects of supply and transport disequilibrium can explain over 2/3 of the variability in τ^*_{rs50} (Table 1). Note that τ^*_c and τ^*_{rs50} are assumed to be interchangeable for these model fits. The procedure used for estimating best-fit model parameters for Eq. (5) and (7) was different from that described above. The fact that these models are differential equations prevented the use of nonlinear multiple regressions. Instead, a brute-force approach was done of incrementally stepping through a wide range of parameter space of k, κ_{dep} and κ_{ent}, and finding the combination of parameters that gave the smallest RMSD. The calculations of τ^*_{rs50} through time were started at τ^*_{rs50}=0.036 at t=0, which is consistent with the experiments, and also is the τ^*_{rs50} proposed by Wilcock and Crowe (2003) in the absence of sand dependence.

Interestingly, model fits using $A_r = D_{s50}/\sigma$ are not substantially different from A_r=1, and R^2=0.69 is the same (Fig. 5). Table 1 includes three additional regressions not shown on Fig. 5 because the fits overlap almost completely with those already shown. $A_r = D_{s50}/D_{s84}$ was tried, because the inverse ratio D_{s84}/D_{s50} represents the degree of armoring in the analysis of τ^*_c supply dependence by Recking (2012). $A_r = 2D_{s50}/(D_{s84} - D_{s16})$ was also tried as a measure of the normalized GSD width. Finally, parameters were estimated for dimensional $\partial q_s/\partial x$ (Eq. 5). Because these variants do not substantially improve τ^*_c model fits, we use the simplest dimensionally consistent model (Eq. 7 with A_r=1) in the analysis below.

Earth Surf. Dynam. Discuss., doi:10.5194/esurf-2015-52, 2016
Manuscript under review for journal Earth Surf. Dynam.
Published: 19 January 2016

3.3 Influence of τ_c^* evolution on morphodynamics

3.3.1 Morphodynamic model development

Next, an idealized morphodynamic model demonstrates how the proposed τ_c^* relations influence the evolution of channel reach profiles, focusing on reach slopes and timescales of adjustment. Because the modeling goal is to isolate and understand effects of evolving τ_c^*, the underlying model is arguably the simplest reasonable representation of morphodynamic feedback. Inspired by G. Parker's Morphodynamics e-book, the model describes a channel reach in which slope evolves through aggradation and degradation. The downstream boundary elevation is fixed (constant base level). Sediment transport and bed elevation are modeled using Eq. (1) and (4) with a single grain diameter (D). Unit water discharge q_w is similarly held constant for simplicity. Upstream sediment supply (q_{sfeed}) is imposed, and is varied in simulations below to drive channels to new steady states. Relationships among flow depth, depth-averaged velocity and discharge are imposed by assuming that hydraulic roughness remains constant, parameterized though a Darcy-Weisbach hydraulic friction coefficient:

$$f = \frac{8gq_w S}{U^3} \tag{15}$$

For a given discharge this allows both U and h to be determined:

$$U = \frac{q_w}{h} \tag{16}$$

$$h = q_w^{2/3}\left(\frac{f}{8gS}\right)^{1/3} \tag{17}$$

Although not presented, simulations were also done in which the relation between U and h was determined by instead holding Froude number ($Fr = U/\sqrt{gh}$) constant (Grant, 1997). While f changes systematically with slope in this scenario, resulting trends in reach slope adjustment and response timescales are substantively the same as shown below for constant f, suggesting little sensitivity to the underlying hydraulic closure assumptions.

Earth Surf. Dynam. Discuss., doi:10.5194/esurf-2015-52, 2016
Manuscript under review for journal Earth Surf. Dynam.
Published: 19 January 2016

Two model variations are compared: in the "Exner-only" morphodynamic model, τ_c^* is held constant. In the "Exner+ τ_c^*" variant, τ_c^* evolves through time following Eq. (7). At equilibrium, channel slope can be predicted by combining Eq. (1), (2), (9) and (17):

$$S_{eq} = \frac{2.83}{q_w}\left(\frac{g}{f}\right)^{1/2} D^{3/2}\left(\frac{\rho_s}{\rho}-1\right)^{3/2}\left[\left(\frac{q_s^*}{3.97}\right)^{2/3}+\tau_c^*\right]^{3/2} \quad (18)$$

For a given discharge, Eq. (18) indicates that both sediment supply and the threshold of motion influence steady-state morphology (slope).

Away from equilibrium, rates of bed elevation change along a river profile should depend not only on the sediment flux at a given channel cross section, but also on the average velocity at which grains move downstream. This control has occasionally been ignored in previous models of profile evolution. In my model, it is crudely incorporated by assuming that average bedload velocity is a consistent fraction of water velocity, broadly consistent with previous findings that bedload velocities are proportional to shear velocity (e.g., Martin et al., 2012). The modeling timestep is set to be equal to the time it takes sediment to move from one model node (bed location) to the next, and is adjusted during simulations. While this approach makes the temporal evolution of channel changes internally consistent within the model, timescales for morphological response will be much shorter than actual adjustment times in field settings because flood intermittency is not included (so the model as implemented is always at a constant flood discharge). In addition, the upstream sediment supply is imposed in the model, while in natural settings hillslope-floodplain-channel coupling could greatly affect q_{sfeed} over time if significant aggradation or downcutting took place.

Table 2 provides parameters used for morphodynamic modeling. Although the highly simplified model is not intended for quantitative field comparisons, variables D (D_{s50}=50 mm), f (0.1), and q_w (1 m^2/s) were chosen to be broadly consistent with a moderate (≈2-3 year peak discharge recurrence interval) bedload-transporting flood in Reynolds Creek, Idaho (Olinde and Johnson, 2015). Reynolds creek is a snowmelt-dominated channel with reach slopes that vary widely from ~0.005 to 0.07. In an instrumented reach with a slope of 0.02, Olinde (2015) used RFID-tagged tracers and channel-spanning RFID antennas to measure $\tau_{rs50}^* \approx 0.06$. A constant τ_c^*=0.06 is used for the Exner-only only models, while τ_c^*=0.06 is

Earth Surf. Dynam. Discuss., doi:10.5194/esurf-2015-52, 2016
Manuscript under review for journal Earth Surf. Dynam.
Published: 19 January 2016

399 used as the initial condition for Exner+τ_c^* models with evolving τ_c^*. Upstream sediment feed
400 rates (q_{sfeed}) were not constrained by field data, and were chosen to provide reasonable
401 modeled slopes. Exponents κ_{dep} and κ_{ent} used the experimental calibrations, while k were
402 chosen so that changes in τ_c^* occurred over the same range of timescales as topographic
403 adjustments, to better illustrate the interplay of variables in morphodynamic evolution.

404 ### 3.3.2 Morphodynamic model results

405 Fig. 6 compares how the Exner-only (constant τ_c^*) and Exner+τ_c^* (evolving τ_c^*)
406 models respond to an increase in sediment supply. The initial condition is a channel at
407 equilibrium (q_{sout}=q_{sin}=q_{sfeed}). At t=0, sediment supply is increased by a factor 5. The τ_c^*-
408 evolution model aggrades to a new equilibrium slope that is lower than the constant τ_c^* model.
409 This occurs because $\partial q_s / \partial x < 0$ causes evolving τ_c^* to decrease over time, progressively
410 increasing transport efficiency (i.e., higher transport rates at a lower slope) compared to
411 constant τ_c^*=0.06 (Fig. 7). Feedback causes the reverse effect in response to a decrease in
412 q_{sfeed} (Fig. 7). For the Exner+τ_c^* model, τ_c^* progressively increases as slope decreases,
413 leading the channel to re-equilibrate both sooner and at a higher slope.

414 An equilibrium timescale (t_{eq}) is measured as the amount of time it takes from a
415 supply perturbation (t=0 in these models) to having the slope adjust to be within 0.0001 of its
416 asymptotic equilibrium slope. In Fig. 7, t_{eq} are substantially longer for the Exner-only models
417 (constant τ_c^*) than for the otherwise equivalent Exner+τ_c^* models. Slope and τ_c^* adjust at the
418 same time in the Exner+τ_c^* models, and influence transport in the same direction. For
419 example, an increase in q_{sfeed} leads to aggradation, in turn increasing q_s^* by both increasing
420 slope and decreasing τ_c^* and (Eq. 1, 5). Both factors adjusting enable equilibrium to be
421 reached sooner.

422 Fig. 8a confirms, over a q_{sfeed} range of two orders of magnitude, that equilibrium
423 slopes changes less for the Exner+τ_c^* model than for Exner-only. The ratio of these
424 equilibrium slopes illustrates the magnitude of the change, where "S_{eq} ratio" is S_{eq} for
425 Exner+τ_c^* divided by Exner-only S_{eq} (Fig. 8b). An order-of-magnitude decrease in q_{sfeed}

Earth Surf. Dynam. Discuss., doi:10.5194/esurf-2015-52, 2016
Manuscript under review for journal Earth Surf. Dynam.
Published: 19 January 2016

caused Exner+ τ_c^* S_{eq} to be between roughly 24% and 36% larger than Exner-only S_{eq}, while an order-of-magnitude increase in q_{sfeed} led to Exner+ τ_c^* roughly 20% smaller than the constant-τ_c^* model. Calculations are shown for several values of scaling factor *k*. A larger *k* means that τ_c^* increases or decreases more rapidly for a given amount of aggradation or degradation (Eq. 7), which in general enables a new equilibrium to be reached with a smaller change in slope.

Equilibrium timescales are quite sensitive to *k* as well as to sediment supply rate (Fig 8c). Similar to the S_{eq} ratio, the "t_{eq} ratio" is Exner+ τ_c^* t_{eq} divided by Exner-only t_{eq} (Fig. 8d). There is an asymmetry in equilibrium times for aggradation vs. degradation; in general the difference between Exner-only and Exner+ τ_c^* is somewhat smaller during bed aggradation, and the difference decreases with increasing q_{sfeed}. Interestingly, the highest *k* (2.8E-5) results in a threshold-like response where the t_{eq} ratio rapidly increases from roughly 0.01 to 0.8 (Fig. 8d). This change occurred at the feed rate at which τ_c^* "bottomed out", i.e. reached its minimum possible value ($\tau_c^* \approx \tau_{c\min}^*$=0.02) before the equilibrium slope had been attained (Fig. 8e). At that point, τ_c^* could no longer act as a buffer to reduce more gradual slope changes.

Finally, Fig. 9 shows that the spatial as well as temporal evolution of τ_c^* can influence river profiles. The models are the same as in Fig. 6. At *t*=0, the feed rate *into the upstream-most node* (node 1, 0 km) increases by a factor of 5. Thus the upstream end feels the flux perturbation both sooner and more strongly than downstream nodes. Aggradation from the supply perturbation increases upstream slopes first. In the Exner-only model, downstream slopes gradually catch up (Fig. 9a): because τ_c^* stays constant, every location along the channel eventually asymptotes to the single slope required to transport the new q_{sfeed} at the given discharge. However, for evolving τ_c^*, enhanced upstream aggradation caused upstream τ_c^* to decrease both more rapidly and to lower values than downstream nodes. Spatial differences in τ_c^* persisted at equilibrium, resulting in spatial variations in equilibrium slope (Exner+ τ_c^*; Fig. 9b, 9c).

Earth Surf. Dynam. Discuss., doi:10.5194/esurf-2015-52, 2016
Manuscript under review for journal Earth Surf. Dynam.
Published: 19 January 2016

4 Discussion

In this section, the dependence of τ_c^* on sediment supply is compared to previous work. τ_c^* evolution is identified as a negative feedback on morphologic change that can impart a memory of previous channel "states" to the system. The physical significance of τ_c^* variability is interpreted in terms of steady-state slope variability along a natural channel. Finally, τ_c^* is interpreted as a channel state variable, analogous to temperature in thermodynamics. By incorporating τ_c^* evolution, landscape evolution models may be able to implicitly account for morphodynamic variables including roughness and form drag.

4.1 Comparison to previous work

Recking (2012) compared long-term bed load monitoring records from steep natural channels (>5% slope) to differences in sediment supply interpreted from aerial photographs of surrounding hillslopes. Channels with higher supply rates had higher transport rates for a given shear stress, suggesting a dependence of transport thresholds on supply. Recking (2012) proposed models for putting end-member bounds on reference stress for the cases of very high sediment supply (τ_{mss}^*) and very low sediment supply (τ_m^*) in steep mountain channels:

$$\tau_{mss}^* = (5S + 0.06)\left(\frac{D_{84}}{D_{50}}\right)^{-1.5} \quad (19)$$

$$\tau_m^* = (5S + 0.06)\left(\frac{D_{84}}{D_{50}}\right)^{4.4\sqrt{S}-1.5} \quad (20)$$

The ratio D_{84}/D_{50} is intended to represent the degree of armoring, which varies with sediment supply (e.g., Dietrich et al., 1989). It should be noted that these reference stresses parameters were calibrated to describe transport of the D_{84} grain size (rather than D_{50}) using a different transport model (Recking, 2012). Nonetheless, τ_{mss}^* and τ_m^* were shown to be fairly comparable to typical nondimensional threshold such as τ_c^* in Eq. (1). Fig. 10 compares Eq. (19) and (20) to the experimental constraints on τ_{rs50}^*. For the most part, τ_{mss}^* and τ_m^* do bound τ_{rs50}^*. The low supply bound τ_m^* is roughly 3 times larger than the experimental

Earth Surf. Dynam. Discuss., doi:10.5194/esurf-2015-52, 2016
Manuscript under review for journal Earth Surf. Dynam.
Published: 19 January 2016

479 constraints. While τ^*_{mss} is similar in magnitude to τ^*_{rs50} and predicts the decrease during the
480 feed period, the (linear) correlation between τ^*_{mss} and τ^*_{rs50} is weak (R^2=0.13) although
481 statistically significant (p=3E-5). Nonetheless, given that threshold of motion uncertainties
482 are typically large, Eq. (19) arguably provides a surprisingly good independent prediction of
483 our experimental disequilibrium transport data, based on experimental slope, D_{84} and D_{50}.

484 Bunte et al. (2013) also interpreted that lower τ^*_c corresponded to looser beds caused
485 by higher rates of sediment supply from upstream, and noted that the stability of bed particles
486 can be qualitatively assessed in the field while doing pebble counts. Yager et al. (2012b)
487 demonstrated that in-channel sediment availability varied inversely with the degree of boulder
488 protrusion. While the τ^*_c-evolution model is not inconsistent with high sediment supply rates
489 correlating with low τ^*_c, Eq. (5) and (7) say something different: τ^*_c does not directly increase
490 or decrease with supply, but rather with the history of sediment supply relative to transport
491 capacity over time. If q_{sin} equals q_{sout}, τ^*_c will remain constant regardless of whether q_{sin} is
492 high or low.

493 **4.2 Negative feedback and asymmetric approaches to equilibrium**

494 The evolution of τ^*_c acts as a negative feedback because it reduces the
495 morphodynamic response to perturbations. Reach slopes and τ^*_c both change in the direction
496 that brings transport back towards equilibrium, allowing smaller slope changes to accomodate
497 supply changes (Fig. 6, 7, 8a,b, 9). However, as with other buffered systems, there is a limit to
498 how large of a perturbation can be accommodated by τ^*_c (as illustrated by k=2.8E-5 in Fig.
499 8c,d,e). The amount of possible τ^*_c change depends on how close the τ^*_c is to the threshold
500 boundaries, i.e. $\tau^*_{c\min}$ or $\tau^*_{c\max}$ (Eq. 5, 7). When changes in τ^*_c are no longer possible (or are
501 asymptotically small) but transport and morphology are not equilibrated, then the time to
502 equilibrium (t_{eq}) increases because only channel morphology can adjust (Fig. 8c, d, e).

503 The experiments suggest that τ^*_c changes faster in response to aggradation than
504 degradation (Fig. 2, 5). This asymmetry is expressed in the best-fit exponents: κ_{dep} is smaller
505 than κ_{ent} for all scenarios tested (Table 1). Note that because $\partial\theta_s/\partial x$ is much smaller than 1
506 (i.e, spatial changes in bed elevation are small compared to the horizontal distance the change

Earth Surf. Dynam. Discuss., doi:10.5194/esurf-2015-52, 2016
Manuscript under review for journal Earth Surf. Dynam.
Published: 19 January 2016

is measured over), the smaller exponent (κ_{dep}) corresponds to a larger change in τ_c^* for a given $\partial\theta_s/\partial x$ (Eq. 7). Thus, aggradation is more efficient at decreasing τ_c^* than degradation is at increasing τ_c^*, for a given increment of sediment thickness (θ_s). But why then does Fig. 8c indicate, for the Exner+τ_c^* model, that equilibrium timescales are longer for aggradation (q_{sfeed} / initial q_{sfeed} > 1) than for degradation? The explanation is that the equilibrium timescale does not *only* depend on the exponents, but also on how much total aggradation or degradation occurs to attain equilibrium, and how quickly sediment enters or exits the reach to enable that aggradation or degradation. More slope change occurred during aggradation than degradation for these particular Exner+τ_c^* models (Fig. 8a), even though τ_c^* also tended to change by more during aggradation than degradation (Fig. 8e).

In the experiments, average slopes changed very little in response to changes in sediment supply and transport disequilibrium, while grain size and bed surface roughness changed much more (Fig. 2). Because grain size changes were accounted for (by the W&CM) in determining experimental τ_{rs50}^* (Fig. 3), roughness and other unquantified mechanisms (such as grain interlocking) are interpreted to have caused the τ_{rs50}^* evolution. What does this suggest for *k*, which scales how much τ_c^* changes for a given amount of aggradation or degradation? The best-fit *k* to the collective experiments was 2.83E-3 s^{-1}, which reflects the rapid adjustment of τ_c^* compared to slope changes (Fig. 5, Table 1, Eq 7). In contrast, the morphodynamic modeling used *k* values adjusted to be 2 to 3 orders of magnitude smaller, so that the response to a perturbation in supply would involve non-negligible changes in slope (the only morphologic variable in the simple morphodynamic model) as well as in τ_c^*. Higher values of *k* in the morphodynamic model cause τ_c^* to adjust more rapidly and slope to adjust less (Fig. 8).

4.3 Memory, morphologic variability, and Reynolds Creek

An implication of τ_c^* evolving with reach morphodynamics is that local channel form can retain "memories" of previous conditions, which can influence local responses to subsequent forcing. In Fig. 9b and 9c, an increase in supply led to the temporal and spatial evolution of τ_c^*, which in turn caused spatial variations in equilibrium slope. Upstream

Earth Surf. Dynam. Discuss., doi:10.5194/esurf-2015-52, 2016
Manuscript under review for journal Earth Surf. Dynam.
Published: 19 January 2016

535 reaches acted as filters of the supply perturbation to downstream reaches (here, "reach" refers
536 to a small fraction of the total modeled longitudinal distance). In contrast, slope variability
537 developed during the transient adjustment period when τ_c^* remained constant, but all reaches
538 evolved to the same equilibrium slope required to transport the new supply (Fig. 9a).

539 Natural river channels inevitably exhibit morphologic variability at reach scales. For
540 example, although the longitudinal profile of Reynolds Creek appears smoothly concave over
541 a spatial scale of 10 km (Fig. 11a), there is substantial slope variability when calculated for
542 100 m reaches (Fig. 11b). This 100 m averaging scale was chosen for the following analysis
543 because it is sufficiently large to plausibly be used for landscape evolution modeling, while
544 small enough to capture slope variability along a profile.

545 How much variability in reach slope could be explained by commonly observed
546 variability in τ_c^* (e.g., Fig. 1)? Eq. (18), which assumes equilibrium transport, can be
547 rearranged to predict transport thresholds for a given slope, water discharge and
548 nondimensional sediment flux:

549 $$\tau_c^* = \frac{(q_w S)^{2/3}}{2D\left(\frac{\rho_s}{\rho}-1\right)}\left(\frac{f}{g}\right)^{1/3} - \left(\frac{q_s^*}{3.97}\right)^{2/3} \quad (21)$$

550 Fig. 11c compares a histogram of compiled τ_c^* (Fig. 1) to a histogram of calculated τ_c^* using
551 Eq. (21), based on the reach slopes along Reynolds Creek (Fig. 11b). Fig. 11d compares
552 slope predictions calculated using Eq. (18) and the τ_c^* compilation (Fig. 1) to the 100 m reach
553 slopes of Reynolds Creek. Although slope can be influenced by many factors, it appears
554 plausible that natural slope variability in part reflects variability in thresholds of motion.
555 While compilations are often assumed to reflect "typical" distributions, there is no reason that
556 the τ_c^* values from Fig. 1 should reflect the particular distribution of τ_c^* for D_{50} in Reynolds
557 Creek. Beyond a field measurement of 0.06 at a particular location, τ_c^* distributions are
558 spatially unconstrained. These calculations also assumed q_s^*=2E-3 because it provided a
559 reasonable overlap of the distributions. Nonetheless, a hypothesis to motivate future work is
560 that systematic and predictable differences in τ_c^* would be found for Reynolds Creek reaches
561 that overlap with the τ_c^*-predicted slope distribution, because slope variations dominantly
562 reflect adjustments to transport the sediment load from upstream. The steeper Reynolds Creek

Earth Surf. Dynam. Discuss., doi:10.5194/esurf-2015-52, 2016
Manuscript under review for journal Earth Surf. Dynam.
Published: 19 January 2016

slopes are interpreted to reflect additional slope influences, such as the abundance of boulders. Olinde (2015) did extensive point counts to measure surface GSDs over 11 reaches along Reynolds Creek, and found that coarse size percentiles (e.g. D_{84}) varied greatly but D_{50} had less variation. Larger boulders tend to be immobile, while the more mobile grains (e.g. D_{50}) are transported through all of the reaches (e.g., Yager et al., 2007).

Previous studies have explored the slope dependence of τ_c^* by mechanistically explaining mean trends (Prancevic and Lamb, 2015; Lamb et al., 2008) (Fig 1). In addition, Fig. 3, 9 and 11 suggest that τ_c^* variability can be both meaningful and physically inherent to bedload transport, because slope and τ_c^* inevitably evolve together in response to discharge and sediment supply. In nature, spatially and temporally-averaged morphodynamic equilibrium will reflect "channel-forming" discharges and a representative sediment supply from upstream, but floods, local supply perturbations and history add to local variability in τ_c^* and morphology.

4.4 State function framework for modeling morphodynamics

I argue that τ_c^* is an important state variable for gravel-bed channels, and outline a possible state function approach for modeling the morphodynamic evolution of channels. The term "bed state" has long been informally used to describe collective aspects of local channel morphology, such as surface GSD and armoring and clustering, that change with relative ease and influence transport rates (e.g., Church, 2006; Gomez and Church, 1989). Although explicitly describing τ_c^* evolution and related river feedbacks in terms of state and path functions may be novel (to my knowledge), this approach is in many ways conceptually equivalent to the description by Phillips (2007) of landscape evolution and form in terms of system states and the importance of history, and similar to other works that describe and generalize complex channel morphology process and response feedbacks (e.g., Fonstad, 2003; Phillips, 2011, 2009; Chin and Phillips, 2007; Phillips, 1991; Stark and Stark, 2001; Yanites and Tucker, 2010).

State variables or state functions are integral to many disciplines, including control systems engineering and thermodynamics. For example, temperature, pressure, enthalpy and entropy are some of the many thermodynamic state variables. By definition state variables are path-independent (Oxtoby et al., 2015). For example, temperature (T) describes the amount

Earth Surf. Dynam. Discuss., doi:10.5194/esurf-2015-52, 2016
Manuscript under review for journal Earth Surf. Dynam.
Published: 19 January 2016

of thermal energy per unit of a material. A change in temperature of the material depends on its initial and final states alone (i.e., $\Delta T=T_2-T_1$), but does not depend on the path, i.e. the history of temperatures in between times t_2 and t_1. In contrast, heat--the flow (transfer) of thermal energy--is a path function (or process function), not a state variable. Heat flow between bodies is both controlled by and changes the temperature (the state) of those bodies, but the amount of total heat transferred does depend on the path. Three other points about state functions are relevant. First, state functions are often interrelated rather than independent of one another. For example, Gibbs free energy is state function calculated from temperature, enthalpy and entropy (Hemond and Fechner, 2014). Second, although traditional state functions are technically only defined for systems at equilibrium, in practice they are valid and useful approximations of gradually evolving systems (e.g., Kleidon, 2010). Third, the evolution of systems involving multiple state variables are usually described with coupled differential equations.

Channel morphodynamics could be described by a similar framework of state and path functions. Analogous to heat, the cumulative discharges of both water and sediment are path functions that drive bed state evolution. Channel morphology can be described by numerous bed state variables, including but not limited to surface GSD, slope, width, depth, bed roughness, surface grain clustering, interlocking, overlap and imbrication, and finally τ_c^*. Analogous to temperature, τ_c^* is a state variable because, for example, a change in τ_c^* of 0.01 (from say 0.04 at t_1 to 0.05 at t_2) does not depend on the progression of values in between. However, the amount of sediment transported between times t_1 and t_2 does depend on the history of τ_c^*, and also influences the history of τ_c^* (Eq. 5, 7).

It is worth noting that entropy is the state variable perhaps used most often to characterize channel systems (e.g., Chin and Phillips, 2007; Leopold and Langbein, 1962; Rodriguez-Iturbe and Rinaldo, 1997). Entropy is often used to provide a closure for underconstrained sets of equations, by assuming that geomorphic and other systems inherently maximize their entropy at equilibrium (Kleidon, 2010; Chiu, 1987). A limitation of some maximum-entropy landscape models is that physically-based surface processes are not always explicitly modeled, making results difficult to validate and less useful for exploring landscape responses to perturbations or behavior away from steady state, even if they can

Earth Surf. Dynam. Discuss., doi:10.5194/esurf-2015-52, 2016
Manuscript under review for journal Earth Surf. Dynam.
Published: 19 January 2016

create reasonable-looking equilibrium morphologies (Paik and Kumar, 2010). In contrast, state function τ_c^* has a clear process-based meaning.

How could a state function framework improve morphodynamic modeling and incorporate subgrid-scale channel feedbacks into broader landscape evolution models? Simplicity is important: the most insight is often gained by using the simplest possible model that can still capture essential feedbacks over spatial and temporal scales of interest. As described in the introduction, previous work has shown that τ_c^* is influenced by many characteristics of the surrounding bed surface. In other words, τ_c^* is closely related to other bed state variables. It would probably be impractical to develop or apply a "complete" τ_c^* model that explicitly incorporated separate state variables for multiple known controls on τ_c^*. Instead, the τ_c^* evolution equation (Eq. 5, 7) attempts to strike a balance between predicting process in a physically justifiable (but empirically calibrated) way, while remaining broadly applicable. It could similarly be impractical to apply a "complete" reach-scale morphodynamic model that explicitly parameterized myriad feedbacks using every corresponding bed state variable. Instead, because many bed state variables are not actually independent of τ_c^*, aspects of morphology can be subsumed into evolving τ_c^* for modeling purposes. This is similar to the channelization approach of Stark and Stark (2001). For example, in the experiments the bed responded to transport disequilibrium primarily by changing roughness but not slope. However, roughness was not an explicit, separate variable in the best-fit τ_{rs50}^* calculations. Instead, some effects of evolving roughness and other bed state controls (imbrication, clustering) on transport rates became implicitly accounted for in the experimentally calibrated τ_{rs50}^* ($\approx \tau_c^*$). The best-fit model parameters (k, κ_{dep}, κ_{ent}; Eq. 7; Table 1) would presumably change if a separate differential equation was developed to explicitly describe another state variable that is currently implicit in τ_c^*, such as bed roughness. It is also important to note that bed roughness could have other effects, such as modifying hydraulic roughness, that are not implicitly captured by τ_{rs50}^* (Schneider et al., 2015b).

Earth Surf. Dynam. Discuss., doi:10.5194/esurf-2015-52, 2016
Manuscript under review for journal Earth Surf. Dynam.
Published: 19 January 2016

4.5 Form drag vs. parsimony

Calculations of best-fit τ^*_{rs50} and transport rates used total shear stress (Eq. 9), rather than partitioning stress into form drag and a lower effective stress used for calculating transport rates (skin friction). Although not a state variable, form drag is physically justifiable because larger clasts that protrude higher into the flow (e.g. stable boulders) tend to account for a disproportionate amount of the total stress through drag, turbulence generation and pressure gradients. Form drag corrections have been incorporated into many transport models to enable reasonable transport rates to be calculated using τ^*_c values typical of systems without form drag (e.g., Rickenmann and Recking, 2011; David et al., 2011; Yager et al., 2012a). Conversely, another common approach is simply to use higher τ^*_c (e.g., Bunte et al., 2013; Lenzi et al., 2006), consistent with acknowledging that τ^*_c can be a physically meaningful fitting parameter to predict transport. Using field data on steep channel gravel transport, Schneider et al. (2015a) recently compared transport predictions based on (a) form drag corrections and (b) higher reference stresses. For the most part they found that either approach could provide similar accuracy. They also noted that "uncertainties in predicted transport rates remain huge (up to roughly 3 orders of magnitude)" (Schneider et al., 2015a), and suggested that factors including supply effects may account for remaining discrepancies. Although beyond the scope of the present analysis, form drag effects could be separated from best-fit τ^*_{rs50} by using a calculated skin friction stress rather than total stress. However, doing so would add extra uncertainty to the shear stresses, while still not accounting for effects of sediment supply. Implicitly subsuming form drag into τ^*_c arguably provides a simpler and more parsimonious approach for modeling transport and morphodynamics.

5 Conclusions

Flume data and a corresponding model demonstrate that nondimensional critical shear stress (τ^*_c) evolves through time as a function of sediment transport disequilibrium. Net erosion tends to increase local τ^*_c (reducing transport rates), while net deposition tends to decrease τ^*_c (increasing transport rates). This τ^*_c dependence on sediment supply relative to transport capacity can plausibly explain much of the ~order-of-magnitude variability almost inevitably observed in transport threshold data (Fig. 1). This view contrasts with a more

Earth Surf. Dynam. Discuss., doi:10.5194/esurf-2015-52, 2016
Manuscript under review for journal Earth Surf. Dynam.
Published: 19 January 2016

conventional approach in which thresholds of motion are assumed to remain constant in time, and τ_c^* variability is treated as noise rather than interpretable signal.

Flume experiments measured sediment transport and channel response away from equilibrium, as beds stabilized and responded to pulses of gravel. Because studies of transport disequilibrium are relatively uncommon, much of our ability to predict transport rates implicitly assumes steady state conditions. The experiments explore a parameter space typical of step-pool morphologies, with steep slopes (8-12%), flow depths comparable to the coarsest grain size fractions, and mixed grain size transport (Johnson et al., 2015). While τ_c^* has physical meaning, it is also a fitting parameter that depends on the choice of sediment transport model. The experimental data are fit by the Wilcock and Crowe (2003) model for mixed grain size transport, to back-calculate both hiding function exponents and transport thresholds (which in this model are nondimensional reference stresses, τ_{rs50}^*). The Wilcock and Crowe (2003) hiding function provides a good prediction of our data (including different exponents for relatively small and large grains), supporting its applicability to steep channels.

A new differential equation is proposed for predicting the temporal evolution of τ_c^* as a function of $\partial q_s / \partial x$ (Eq. 5-7). After empirically fitting three model parameters, this τ_c^*-evolution equation can explain nearly 70% of the variability in experimental τ_c^*. We incorporate the τ_c^*-evolution equation into a simple model for channel slope evolution. Changes in τ_c^* are negative feedbacks on morphodynamic response, because not only slope but also τ_c^* evolve when perturbed. Evolving τ_c^* also reduces response timescales, allowing channels to more rapidly adjust to new conditions. In addition, spatial and temporal variations in sediment supply can lead to reaches becoming equilibrated over a range of slopes, because τ_c^* also influences the equilibrium slope.

Finally, τ_c^* is interpreted to be a state variable for fluvial channels. State functions and path functions are fundamental to many disciplines such as thermodynamics, because they allow the evolution of systems to be calculated. The same should be true for channels; sediment transport is to heat as τ_c^* is to temperature. More broadly, conceptualizing morphodynamic and landscape evolution models in terms feedbacks among evolving state

Earth Surf. Dynam. Discuss., doi:10.5194/esurf-2015-52, 2016
Manuscript under review for journal Earth Surf. Dynam.
Published: 19 January 2016

variables and path functions may improve our ability to predict landscape responses to land use, climate change and tectonic forcing.

Acknowledgements

I thank A. Aronovitz for conducting the flume experiments, W. Kim for aiding in the experimental design, L. Olinde for Reynolds Creek analysis and helpful discussions, and M. Lamb and J. Prancevic for sharing their τ_c^* data compilation. I also thank the kind-hearted reviewers and editor. Support came from NSF grant EAR-1053508.

Appendix 1 List of variables

A_r	Dimensionless parameter for incorporating grain size or roughness ratios in Eq. (7) [1]
b	Dimensionless hiding function exponent; either described by Eq. 13 or fit as a single value [1]
B	Dimensionless "feedback factor"; Eq. 6 [1]
c_1, c_2, c_3	Dimensionless empirical constants in Eq. (14) [1]
D	Grain diameter, for model cases with a single size only [L]
D_{50}	Median grain diameter [L]
D_{s50}	Median grain diameter of bed surface [L]
D_i	Grain diameter of size class *i* [L]
f	Darcy-Weisbach hydraulic friction coefficient; Eq. (15) [1]
Fr	Froude number [1]
F_i	Areal fraction of grain size class *i* on the bed surface; Eq. 10 [1]
F_s	Areal fraction of sand on the bed surface; Eq. 14 [1]
g	Gravitational acceleration [LT^{-2}]
h	Water depth [L]

Earth Surf. Dynam. Discuss., doi:10.5194/esurf-2015-52, 2016
Manuscript under review for journal Earth Surf. Dynam.
Published: 19 January 2016

733	κ_{dep}	Exponent for net deposition in τ_c^*-evolution models; Eq. (5), (7). [1]
734	κ_{ent}	Exponent for net erosion in τ_c^*-evolution models; Eq. (5), (7). [1]
735	k	Scaling factor for τ_c^* evolution. Dimensions are [1/T] for Eq. (7)
736	λ_p	Bed porosity [1]
737	q_{bi}	Volume sediment flux per unit width of size class *i* in Wilcock and Crowe
738		(2003); Eq. 10 [L^2/T]
739	q_s	Volume sediment flux per unit width [L^2/T]
740	q_s^*	Nondimensional volume sediment flux; Eq. (1) [1]
741	$q_{\sin}$	Sediment flux entering a channel bed area (reach) of interest [L^2/T]
742	q_{sout}	Sediment flux exiting a channel bed area (reach) of interest [L^2/T]
743	q_{sfeed}	Sediment flux entering upstream end of overall model domain [L^2/T]
744	q_w	Volume water discharge per unit width [L^2/T]
745	ρ	Water density [M/L^3]
746	ρ_s	Sediment density [M/L^3]
747	S	Water surface slope [1]
748	S_{eq}	Water surface slope when reach is at equilibrium [1]
749	σ	Bed roughness, measured here as the standard deviation of detrended bed
750		elevations [L]
751	θ_s	Thickness of sediment deposited or eroded in a time interval; Eq. (7) [L]
752	t	Time [T]
753	t_{eq}	Equilibrium timescale for morphological adjustment [T]
754	τ	Shear stress [$MT^{-2}L^{-1}$]
755	τ^*	Shields stress (nondimensional shear stress) [1]

Earth Surf. Dynam. Discuss., doi:10.5194/esurf-2015-52, 2016
Manuscript under review for journal Earth Surf. Dynam.
Published: 19 January 2016

756	τ_c^*	Critical Shields stress (nondimensional critical shear stress) [1]
757	$\tau_{c\max}^*$	Imposed maximum bound for τ_c^* in Eq. (5), (7) [1]
758	$\tau_{c\min}^*$	Imposed minimum bound for τ_c^* in Eq. (5), (7) [1]
759	τ_{mss}^*	High sediment supply nondimensional reference stress end-member bound in
760		Recking (2012) transport model; Eq. (19) [1]
761	τ_m^*	Low sediment supply nondimensional reference stress end-member bound in
762		(Recking, 2012) transport model; Eq. (20) [1]
763	τ_{ri}^*	Reference Shields stress for size class *i*, from Wilcock and Crowe (2003) [1]
764	τ_{rs50}^*	Nondimensional reference Shields stress for surface grains of size D_{s50} [1]
765	U	Depth-averaged water velocity [L]
766	u_τ	Shear velocity; Eq. (10) [L/T]
767	x	Position measured horizontally (distance along channel) [L]
768	z	Position measured vertically (bed elevation)[L]
769	W_i^*	Nondimensional bedload transport rate for grain size class *i*, in Wilcock and
770		Crowe (2003) [1]
771	W&CM	Abbreviation for Wilcock and Crowe (2003) transport model.

772

773 **Captions**

774 Figure 1. Threshold of motion data from both field and experimental studies. A power law
775 regression to these data gives R^2=0.34, indicating that a majority of the variability is not
776 explained by slope alone. Dotted lines indicate common range of τ_c^*=0.03 to 0.06 often
777 assumed for modeling transport, although measured data fall well out of this range. Data
778 have been additionally filtered to only include D_{50} > 2 mm (i.e. gravel) and slopes between
779 0.002 and 0.2. Data were compiled and provided by Prancevic and Lamb (2015), based in
780 part on Buffington and Montgomery (1997), with additional data from Olinde (2015) and
781 Lenzi et al. (2006).

Earth Surf. Dynam. Discuss., doi:10.5194/esurf-2015-52, 2016
Manuscript under review for journal Earth Surf. Dynam.
Published: 19 January 2016

782

783 Figure 2. Flume experiment data (Johnson et al., 2015). a. Sediment transport rate in (Q_{sfeed})
784 and out of the flume. The upstream sediment supply rate was zero other than during the Q_{sfeed}
785 period. Experiment 1 was run for a longer duration than the others but shows similar trends.
786 Note that the outlet Q_s adjusts much faster to match the increase in supply than it does to
787 decrease during periods of no input. b. Median bed surface grain diameters decreased during
788 the feed of finer gravel, and then increase beyond their previous stable bed. c. Flume-
789 averaged bed slopes changed relatively little even as transport rates and D_{50} changed greatly
790 in response to initial bed stabilizing and supply perturbations.

791

792 Figure 3. τ^*_{rs50} fits to the experimental data with the W&CM. ,"W&C fit" uses Eq. (13) to
793 calculate hiding function exponent b, while "Power-law fit" calculates a best-fit b along with
794 τ^*_{rs50}. Error bars give 95% confidence intervals on τ^*_{rs50} based on the regressions; although
795 uncertainty can be broad the trends are clear and consistent. Shaded area indicates times of
796 fine gravel addition (sediment feed) in each experiment.

797

798 Figure 4. Data points are based on power-law fits to exponent b. The W&CM hiding function
799 (Eq. 13) does a good job matching the data, although it was not fit to these points. The first 6
800 measurements of each experiment (roughly the first 10 minutes) were excluded because of
801 large scatter associated with the greatest bed instability. The plot axes reflect the left and
802 right hand sides of Eq. (12), although the plot uses dimensional stresses to be consistent with
803 plots shown in Wilcock and Crowe (2003).

804

805 Figure 5. Best-fit models (Eq. 7 and 14) compared to experimental constraints. The periods
806 of upstream sediment supply (Q_{sfeed}) are indicated by the grey boxes for each experiment.

807

808 Figure 6. Profile evolution, comparing the morphodynamic responses of models with and
809 without threshold evolution. The initial condition is an equilibrium channel with τ^*_c=0.06,
810 upstream sediment supply q_s=1e-3 m^2/s, and an initial equilibrium slope of 0.0147. Sediment

Earth Surf. Dynam. Discuss., doi:10.5194/esurf-2015-52, 2016
Manuscript under review for journal Earth Surf. Dynam.
Published: 19 January 2016

supply is increased 5x at t=0. Lines are each 5 model days apart, and indicate the evolution to a new transport equilibrium.

Figure 7. Slope and critical shear stress evolution, for sediment supply increases (which correspond to Fig. 6 models) and decreases by factors of 5. As in figure 6, t=0 corresponds to an equilibrium condition where the initial slope and initial threshold are consistent with the initial upstream sediment supply. Slope and τ_c^* were averaged over nodes 3-10, leaving out the first and last two nodes because of minor model boundary effects.

Figure 8. Morphodynamic model sensitivity to sediment supply perturbations and *k*. All models started at the same equilibrium condition as shown in Fig. 6 and 7. a. Slope adjustment, normalized by the initial equilibrium slope. The correspondence of Eq. 17 and the morphodynamic model calculations demonstrate that the models did asymptotically attain equilibrium slopes. b. S_{eq} ratio is the ratio of equilibrium slopes of the Exner+τ_c^* model divided by S_{eq} for the Exner-only model, to show the relative affect that that τ_c^* evolution has on equilibrium slopes. c. Equilibrium timescales for model adjustment. d. t_{eq} ratio is the ratio of t_{eq} for the Exner+τ_c^* model divided by t_{eq} for the Exner-only model. Values are lower than 1, indicating that the τ_c^* evolution has a large influence on equilibrium timescales. e. Evolution of τ_c^*.

Figure 9. Spatial and temporal evolution of morphodynamic slopes, for the same models shown in Fig. 6. Slope is initially at equilibrium and responds to the 5x increase in upstream sediment supply at t=0. a. The Exner-only model initially has spatial slope variability, but evolves to a uniform new equilibrium slope. b, c. In the model with evolving τ_c^*, slope and τ_c^* variability persist even at equilibrium.

Earth Surf. Dynam. Discuss., doi:10.5194/esurf-2015-52, 2016
Manuscript under review for journal Earth Surf. Dynam.
Published: 19 January 2016

837 Figure 10. Comparison of experimental and best-fit model constraints on τ^*_{rs50}, compared to
838 proposed constraints for D84 reference stress bounds for low and high sediment supply from
839 Recking (2012).

840

841 Figure 11. Comparison of Reynolds creek and τ^*_c data compilation predictions using Eq. (18)
842 and (21). a. Longitudinal profile based on airborne Lidar (Olinde, 2015). Upstream end
843 (distance=0) is an arbitrary location along the channel (a bridge). Data gap at 730 m is a
844 gauging station weir; the slope steepens downstream of the weir where the valley becomes
845 constricted by bedrock, although the bed remains almost entirely alluvial. b. Slopes
846 calculated (averaged) over 100 m reaches, illustrating reach-scale slope variability. c.
847 Histogram of τ^*_c compilation (data shown in Fig. 1), compared to τ^*_c calculated using Eq.
848 (21), based on Reynolds Creek 100 m slopes (panel b), and assuming q_w=1 m2/s, q^*_s=2e-3,
849 and f=0.1. d. Similar calculation as panel c, but using Eq. 18 to solve for slope as a function
850 of τ^*_c from the Fig. 1 data compilation, and compared to panel b slopes.

851

852

853

854

855

References

Buffington, J. M., Dietrich, W. E., and Kirchner, J. W.: Friction angle measurements on a naturally formed gravel streambed: Implications for critical boundary shear stress, Water Resour. Res., 28, 411-425, doi:10.1029/91wr02529, 1992.

Buffington, J. M., and Montgomery, D. R.: A systematic analysis of eight decades of incipient motion studies, with special reference to gravel-bedded rivers, Water Resources Research, 33, 1993-2029, doi:10.1029/97wr03190, 1997.

Buffington, J. M.: The legend of A. F. Shields, Journal of Hydraulic Engineering-Asce, 125, 376-387, doi:10.1061/(asce)0733-9429(1999)125:4(376), 1999.

Bunte, K., Abt, S. R., Swingle, K. W., Cenderelli, D. A., and Schneider, J. M.: Critical Shields values in coarse-bedded steep streams, Water Resources Research, 49, 7427-7447, doi:10.1002/2012wr012672, 2013.

Buscombe, D., and Conley, D. C.: Effective shear stress of graded sediments, Water Resources Research, 48, 13, doi:10.1029/2010wr010341, 2012.

Chin, A., and Phillips, J. D.: The self-organization of step-pools in mountain streams, Geomorphology, 83, 346-358, doi:10.1016/j.geomorph.2006.02.021, 2007.

Chiu, C. L.: Entropy and Probability Concepts in Hydraulics, Journal of Hydraulic Engineering-Asce, 113, 583-600, 1987.

Church, M.: Bed material transport and the morphology of alluvial river channels, in: Annual Review of Earth and Planetary Sciences, Annual Review of Earth and Planetary Sciences, Annual Reviews, Palo Alto, 325-354, 2006.

David, G. C. L., Wohl, E., Yochum, S. E., and Bledsoe, B. P.: Comparative analysis of bed resistance partitioning in high-gradient streams, Water Resources Research, 47, doi:W07507

10.1029/2010wr009540, 2011.

Dietrich, W. E., Kirchner, J. W., Ikeda, H., and Iseya, F.: Sediment supply and the development of the coarse surface-layer in gravel-bedded rivers, Nature, 340, 215-217, doi:10.1038/340215a0, 1989.

Fonstad, M. A.: Spatial variation in the power of mountain streams in the Sangre de Cristo Mountains, New Mexico, Geomorphology, 55, 75-96, doi:10.1016/s0169-555x(03)00133-8, 2003.

Gilbert, G. K.: The transportation of debris by running water, United States Geological Survey Professional Paper, 86, 1914.

Gogus, M., and Defne, Z.: Effect of shape on incipient motion of large solitary particles, Journal of Hydraulic Engineering-Asce, 131, 38-45, doi:10.1061/(asace)0733-9429(2005)131:1(38), 2005.

Gomez, B., and Church, M.: As assessment of bed load sediment transport formulae for gravel rivers, Water Resources Research, 25, 1161-1186, 1989.

Grant, G. E.: Critical flow constrains flow hydraulics in mobile-bed streams: A new hypothesis, Water Resources Research, 33, 349-358, doi:10.1029/96wr03134, 1997.

Hemond, H. F., and Fechner, E. J.: Chemical fate and transport in the environment, Elsevier, 2014.

897 Jerolmack, D. J.: Causes and effects of noise in landscape dynamics, Eos, Transactions
898 American Geophysical Union, 92, 385-386, doi:10.1029/2011EO440001, 2011.

899 Johnson, J. P. L., Aronovitz, A. C., and Kim, W.: Coarser and rougher: Effects of fine gravel
900 pulses on experimental step-pool channel morphodynamics, Geophys. Res. Lett., 42, 8432-
901 8440, doi:10.1002/2015gl066097, 2015.

902 Kirchner, J. W., Dietrich, W. E., Iseya, F., and Ikeda, H.: The Variability of Critical Shear-
903 Stress, Friction Angle, and Grain Protrusion in Water-Worked Sediments, Sedimentology, 37,
904 647-672, doi:10.1111/j.1365-3091.1990.tb00627.x, 1990.

905 Kleidon, A.: A basic introduction to the thermodynamics of the Earth system far from
906 equilibrium and maximum entropy production, Philos. Trans. R. Soc. B-Biol. Sci., 365, 1303-
907 1315, doi:10.1098/rstb.2009.0310, 2010.

908 Lamb, M. P., Dietrich, W. E., and Venditti, J. G.: Is the critical Shields stress for incipient
909 sediment motion dependent on channel-bed slope?, Journal of Geophysical Research, 113,
910 F02008, doi:10.1029/2007jf000831, 2008.

911 Lenzi, M. A., Mao, L., and Comiti, F.: When does bedload transport begin in steep boulder-
912 bed streams?, Hydrological Processes, 20, 3517-3533, doi:10.1002/hyp.6168, 2006.

913 Leopold, L. B., and Langbein, W. B.: The concept of entropy in landscape evolution, US
914 Government Printing Office Washington, DC, USA, 1962.

915 Mao, L. C.: The effect of hydrographs on bed load transport and bed sediment spatial
916 arrangement, J. Geophys. Res.-Earth Surf., 117, doi:10.1029/2012jf002428, 2012.

917 Marquis, G. A., and Roy, A. G.: Using multiple bed load measurements: Toward the
918 identification of bed dilation and contraction in gravel-bed rivers, J. Geophys. Res.-Earth
919 Surf., 117, 16, doi:10.1029/2011jf002120, 2012.

920 Martin, R. L., Jerolmack, D. J., and Schumer, R.: The physical basis for anomalous diffusion
921 in bed load transport, J. Geophys. Res.-Earth Surf., 117, 18, doi:10.1029/2011jf002075, 2012.

922 Meyer-Peter, E., and Müller, R.: Formulas for bed-load transport, Proceedings, Second
923 Congress, International Association for Hydraulic Structures Research, Stockholm, 39-64,
924 1948.

925 Ockelford, A.-M., and Haynes, H.: The impact of stress history on bed structure, Earth
926 Surface Processes and Landforms, 38, 717-727, doi:10.1002/esp.3348, 2013.

927 Olinde, L.: Displacement and entrainment behavior of bedload clasts in mountain streams,
928 Ph.D., Geological Sciences, The University of Texas at Austin, Austin, Texas, 139 pp., 2015.

929 Olinde, L., and Johnson, J. P. L.: Using RFID and accelerometer-embedded tracers to
930 measure probabilities of bed load transport, step lengths, and rest times in a mountain stream,
931 Water Resources Research, 51, 7572-7589, doi:10.1002/2014wr016120, 2015.

932 Oxtoby, D., Gillis, H., and Butler, L.: Principles of modern chemistry, Cengage Learning,
933 2015.

934 Paik, K., and Kumar, P.: Optimality approaches to describe characteristic fluvial patterns on
935 landscapes, Philos. Trans. R. Soc. B-Biol. Sci., 365, 1387-1395, doi:10.1098/rstb.2009.0303,
936 2010.

937 Paola, C., and Voller, V. R.: A generalized Exner equation for sediment mass balance, J.
938 Geophys. Res.-Earth Surf., 110, F04014, doi:10.1029/2004JF000274., 2005.

939 Parker, G., and Klingeman, P. C.: On Why Gravel Bed Streams Are Paved, Water Resources
940 Research, 18, 1409-1423, doi:10.1029/WR018i005p01409, 1982.

941 Parker, G., Klingeman, P. C., and McLean, D. G.: Bedload size distribution in paved gravel-
942 bed streams, American Society of Civil Engineers, Journal of Hydraulics Division, 108, 1757-
943 1760, 1982.

944 Parker, G.: Surface-based bedload transport relation for gravel rivers, Journal of Hydraulic
945 Research, 28, 417-436, doi:10.1080/00221689009499058, 1990.

946 Phillips, C. B., Martin, R. L., and Jerolmack, D. J.: Impulse framework for unsteady flows
947 reveals superdiffusive bed load transport, Geophys. Res. Lett., 40, 1328-1333,
948 doi:10.1002/grl.50323, 2013.

949 Phillips, J. D.: MULTIPLE-MODES OF ADJUSTMENT IN UNSTABLE RIVER
950 CHANNEL CROSS-SECTIONS, Journal of Hydrology, 123, 39-49, 1991.

951 Phillips, J. D.: Changes, perturbations, and responses in geomorphic systems, Progress in
952 Physical Geography, 33, 17-30, doi:10.1177/0309133309103889, 2009.

953 Phillips, J. D.: Emergence and pseudo-equilibrium in geomorphology, Geomorphology, 132,
954 319-326, doi:10.1016/j.geomorph.2011.05.017, 2011.

955 Powell, D. M., and Ashworth, P. J.: Spatial pattern of flow competence and bed-load transport
956 in a divided gravel-bed river, Water Resources Research, 31, 741-752,
957 doi:10.1029/94wr02273, 1995.

958 Prancevic, J. P., and Lamb, M. P.: Unraveling bed slope from relative roughness in initial
959 sediment motion, J. Geophys. Res.-Earth Surf., 120, 474-489, doi:10.1002/2014jf003323,
960 2015.

961 Recking, A.: Influence of sediment supply on mountain streams bedload transport,
962 Geomorphology, 175, 139-150, doi:10.1016/j.geomorph.2012.07.005, 2012.

963 Richards, K., and Clifford, N.: Fluvial geomorphology: structured beds in gravelly rivers,
964 Progress in Physical Geography, 15, 407-422, doi:10.1177/030913339101500404, 1991.

965 Rickenmann, D., and Recking, A.: Evaluation of flow resistance in gravel-bed rivers through
966 a large field data set, Water Resources Research, 47, doi:10.1029/2010wr009793, 2011.

967 Rodriguez-Iturbe, I., and Rinaldo, A.: Fractal River Networks: Chance and Self-
968 Organization, Cambridge University Press, New York, 1997.

969 Sanguinito, S., and Johnson, J.: Quantifying gravel overlap and dislodgement forces on
970 natural river bars: implications for particle entrainment, Earth Surface Processes and
971 Landforms, 37, 134-141, doi:10.1002/esp.2237, 2012.

972 Schneider, J. M., Rickenmann, D., Turowski, J. M., Bunte, K., and Kirchner, J. W.:
973 Applicability of bed load transport models for mixed-size sediments in steep streams
974 considering macro-roughness, Water Resources Research, 51, 5260-5283,
975 doi:10.1002/2014wr016417, 2015a.

976 Schneider, J. M., Rickenmann, D., Turowski, J. M., and Kirchner, J. W.: Self-adjustment of
977 stream bed roughness and flow velocity in a steep mountain channel, Water Resources
978 Research, 51, 7838-7859, doi:10.1002/2015WR016934, 2015b.

979 Shvidchenko, A. B., and Pender, G.: Flume study of the effect of relative depth on the
980 incipient motion of coarse uniform sediments, Water Resources Research, 36, 619-628,
981 doi:10.1029/1999wr900312, 2000.

982 Sklar, L. S., Fadde, J., Venditti, J. G., Nelson, P., Wydzga, M. A., Cui, Y. T., and Dietrich, W.
983 E.: Translation and dispersion of sediment pulses in flume experiments simulating gravel
984 augmentation below dams, Water Resources Research, 45, doi:10.1029/2008wr007346, 2009.

985 Stark, C. P., and Stark, G. J.: A channelization model of landscape evolution, American
986 Journal of Science, 301, 486-512, doi:10.2475/ajs.301.4-5.486, 2001.

987 Strom, K. B., and Papanicolaou, A. N.: Occurrence of cluster microforms in mountain rivers,
988 Earth Surface Processes and Landforms, 34, 88-98, doi:10.1002/esp.1693, 2009.

989 Venditti, J. G., Dietrich, W. E., Nelson, P. A., Wydzga, M. A., Fadde, J., and Sklar, L.:
990 Mobilization of coarse surface layers in gravel-bedded rivers by finer gravel bed load, Water
991 Resour. Res., 46, doi:10.1029/2009wr008329, 2010.

992 Wilcock, P. R., and Crowe, J. C.: Surface-based transport model for mixed-size sediment,
993 Journal of Hydraulic Engineering-Asce, 129, 120-128, doi:10.1061/(asce)0733-
994 9429(2003)129:2(120), 2003.

995 Wong, M., and Parker, G.: Reanalysis and Correction of Bed-Load Relation of Meyer-Peter
996 and Müller Using Their Own Database, Journal of Hydraulic Engineering, 132, 1159-1168,
997 doi:doi:10.1061/(ASCE)0733-9429(2006)132:11(1159), 2006.

998 Yager, E. M., Kirchner, J. W., and Dietrich, W. E.: Calculating bed load transport in steep
999 boulder bed channels, Water Resources Research, 43, doi:10.1029/2006WR005432, 2007.

1000 Yager, E. M., Dietrich, W. E., Kirchner, J. W., and McArdell, B. W.: Prediction of sediment
1001 transport in step-pool channels, Water Resources Research, 48, doi:10.1029/2011wr010829,
1002 2012a.

1003 Yager, E. M., Turowski, J. M., Rickenmann, D., and McArdell, B. W.: Sediment supply,
1004 grain protrusion, and bedload transport in mountain streams, Geophys. Res. Lett., 39,
1005 doi:10.1029/2012gl051654, 2012b.

1006 Yanites, B. J., and Tucker, G. E.: Controls and limits on bedrock channel geometry, J.
1007 Geophys. Res.-Earth Surf., 115, 17, doi:10.1029/2009jf001601, 2010.

1008

Earth Surf. Dynam. Discuss., doi:10.5194/esurf-2015-52, 2016
Manuscript under review for journal Earth Surf. Dynam.
Published: 19 January 2016

Table 1. Best-fit threshold evolution models

Model type		Best-fit coefficients c_1	c_2	c_3	R^2
"Sand fraction" F_i <2.8 mm, collective best fit	Eq. 14	0.097 (0.057, 0.14)[a]	0.103 (0.009, 0.22)[a]	-5.47 (-16.8, 5.8)[a]	0.13
Units		k 1/s	κ_{dep} 1	κ_{ent} 1	R^2
$\partial\theta_s/\partial x$ model, collective fit	Eq. 7, A_r=1	2.83E-03	0.2	0.4	0.69
$\partial\theta_s/\partial x$ model, Expt 1 fit	Eq. 7, A_r=1	4.12E-02	0.55	0.61	0.52
$\partial\theta_s/\partial x$ model, Expt 2 fit	Eq. 7, A_r=1	4.80E-02	0.55	0.73	0.73
$\partial\theta_s/\partial x$ model, Expt 3 fit	Eq. 7, A_r=1	2.83E-03	0.22	0.41	0.77
$\partial\theta_s/\partial x$ model, Expt 4 fit	Eq. 7, A_r=1	2.75E-02	0.43	0.62	0.75
$\partial q_s/\partial x$ model, collective fit	Eq. 5	9.83E-03[b]	0.25	0.4	0.69
$\partial\theta_s/\partial x$ model, collective fit	Eq. 7, $A_r=D_{s50}/\sigma$	4.17E-03	0.24	0.43	0.69
$\partial\theta_s/\partial x$ model, collectivet fit	Eq. 7, $A_r=D_{s50}/D_{s84}$	4.83E-03	0.23	0.41	0.69
$\partial\theta_s/\partial x$ model, collective fit	Eq. 7, $A_r=2D_{s50}/(D_{s84}-D_{s16})$	3.83E-03	0.23	0.42	0.69

[a]Confidence intervals are +-95%, based on nonlinear multiple regression in Matlab

[b]Units on k for Eq. 5 vary with kent and kdep

Earth Surf. Dynam. Discuss., doi:10.5194/esurf-2015-52, 2016
Manuscript under review for journal Earth Surf. Dynam.
Published: 19 January 2016

Table 2. Morphodynamic Model Parameters

Constant independent variables:

		Units
q_w	1.00	m2/s
D_{50}	50	mm
f	0.1	
h	0.50	m
U	1.99	m/s
λ_p	0.25	
κ_{dep}	0.2	
κ_{ent}	0.4	
τ^*_{cmin}	0.02	
τ^*_{cmax}	0.35	
ρ	1000	kg/m^3
ρ_s	2600	kg/m^3
Total duration	0.5	years
# nodes	12	
node spacing	100	m
$U_{bedload}/U$	0.5	

Initial condition:		Units
q_{sin}, init	1.00E-03	m^2/s
S, init	0.0147	
τ_{cr}*, init	0.06	

Variables changed:		
q_{sin}	1E-5 to 1E-1	m^2/s
k	2.8E-6, 5.7E-6, 2.8E-5	1/s

Earth Surf. Dynam. Discuss., doi:10.5194/esurf-2015-52, 2016
Manuscript under review for journal Earth Surf. Dynam.
Published: 19 January 2016

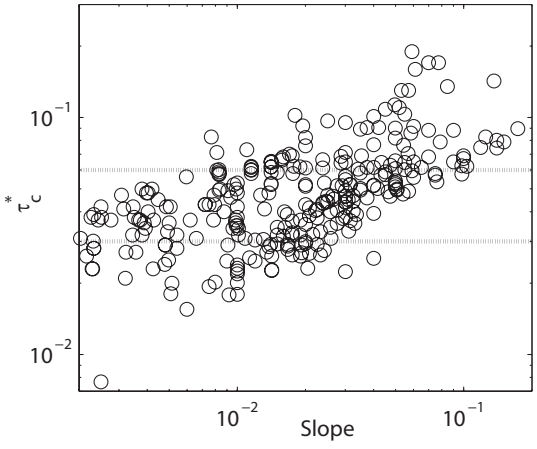

Figure 1. Threshold of motion data from both field and experimental studies. A power law regression to these data gives R^2=0.34, indicating that a majority of the variability is not explained by slope alone. Dotted lines indicate common range of 0.03 to 0.06 often assumed for modeling transport, although measured data fall well out of this range. Data have been additionally filtered to only include D50 > 2 mm (i.e. gravel) and slopes between 0.002 and 0.2. Data were compiled and provided by Prancevic and Lamb (2015), based in part on Buffington and Montgomery (1997), with additional data from Olinde (2015) and Lenzi et al. (2006).

Earth Surf. Dynam. Discuss., doi:10.5194/esurf-2015-52, 2016
Manuscript under review for journal Earth Surf. Dynam.
Published: 19 January 2016

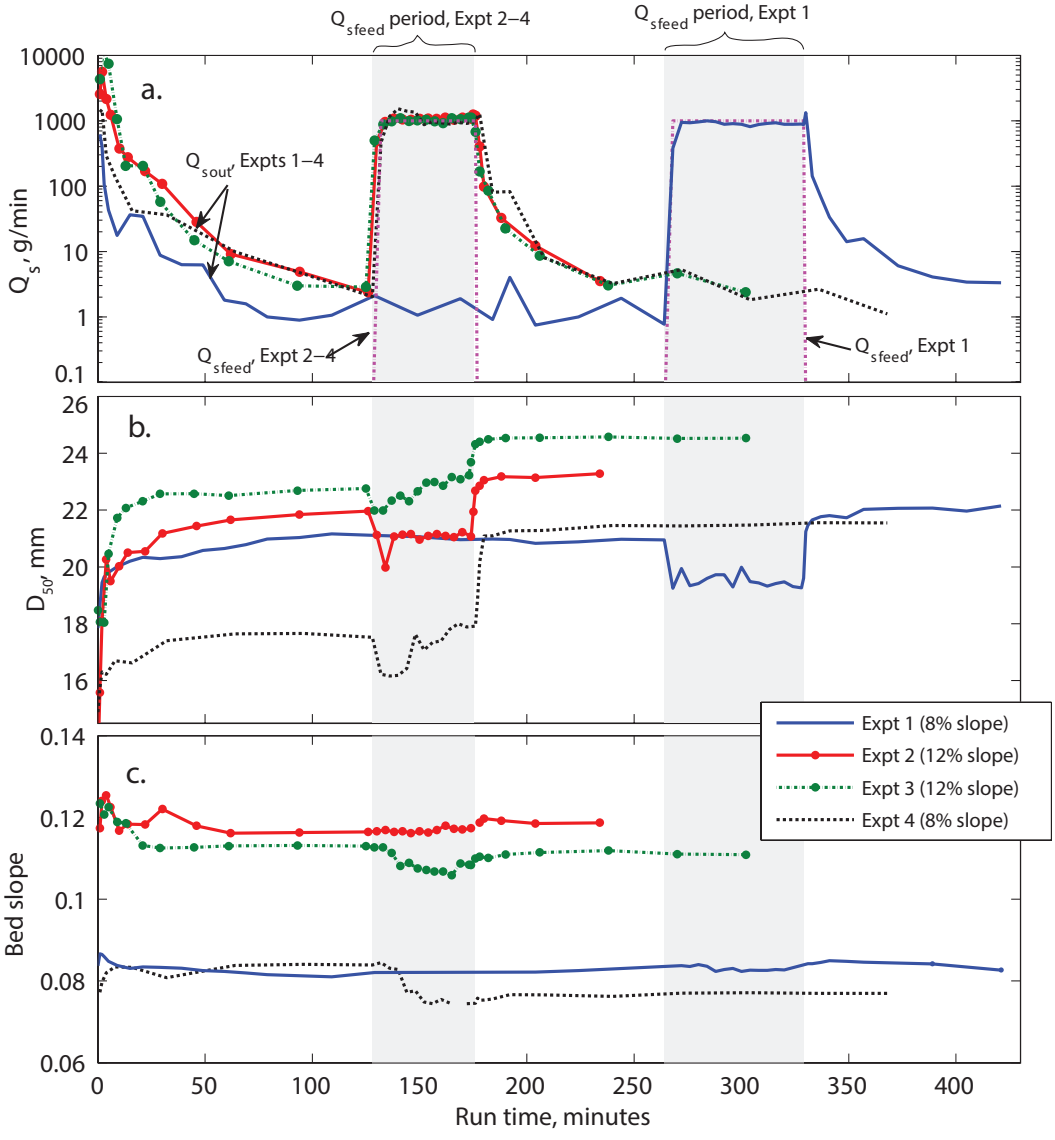

Figure 2. Flume experiment data (Johnson et al., 2015). a. Sediment transport rate in (Q_{sfeed}) and out of the flume. The upstream sediment supply rate was zero other than during the Q_{sfeed} period. Experiment 1 was run for a longer duration than the others but shows similar trends. Note that the outlet Q_s adjusts much faster to match the increase in supply than it does to decrease during periods of no input. b. Median bed surface grain diameters decreased during the feed of finer gravel, and then increase beyond their previous stable bed. c. Flume-averaged bed slopes changed relatively little even as transport rates and D_{50} changed greatly in response to initial bed stabilizing and supply perturbations.

Earth Surf. Dynam. Discuss., doi:10.5194/esurf-2015-52, 2016
Manuscript under review for journal Earth Surf. Dynam.
Published: 19 January 2016

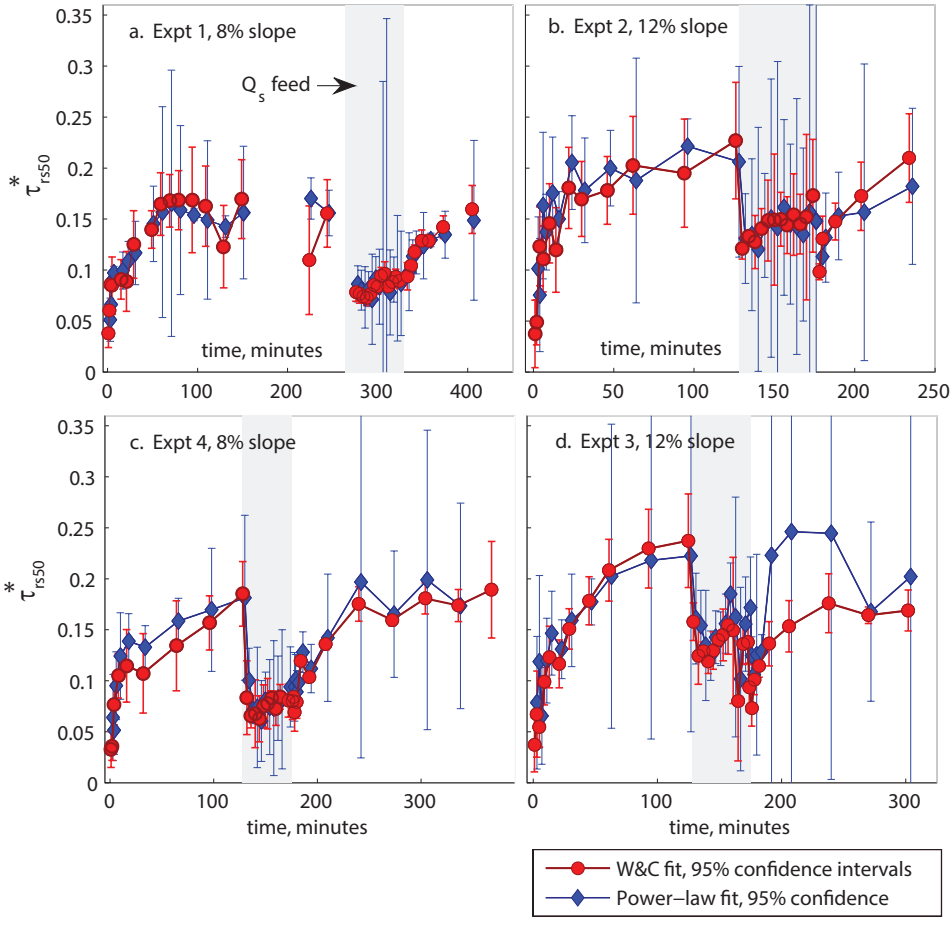

Figure 3. Fits to the experimental data with the W&CM. ,"W&C fit" uses Eq. (13) to calculate hiding function exponent b, while "Power-law fit" calculates a best-fit b along with the threshold parameter. Error bars give 95% confidence intervals based on the regressions; although uncertainty can be broad the trends are clear and consistent. Shaded area indicates times of fine gravel addition (sediment feed) in each experiment.

Earth Surf. Dynam. Discuss., doi:10.5194/esurf-2015-52, 2016
Manuscript under review for journal Earth Surf. Dynam.
Published: 19 January 2016

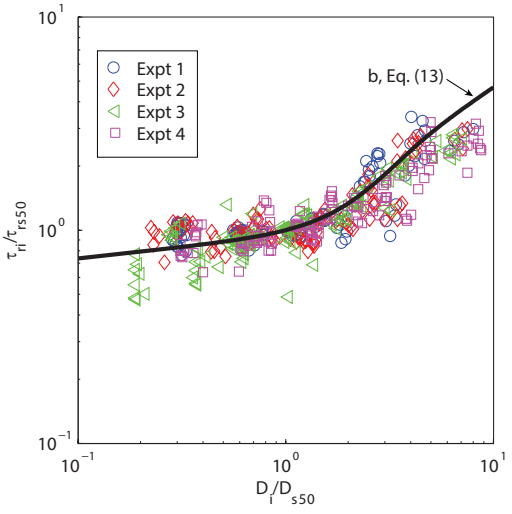

Figure 4. Data points are based on the "Power-law" fits for exponent *b*. The W&CM hiding function (Eq. 13) does a good job matchign the data, although it was not fit to these points. The first 6 measurements of each experiment (roughly the first 10 minutes) were excluded because of large scatter associated with the greatest bed instability. The plot axes reflect the left and right hand sides of Eq. (12), although the plot uses dimensional stresses to be consistent with plots shown in Wilcock and Crowe (2003).

Earth Surf. Dynam. Discuss., doi:10.5194/esurf-2015-52, 2016
Manuscript under review for journal Earth Surf. Dynam.
Published: 19 January 2016

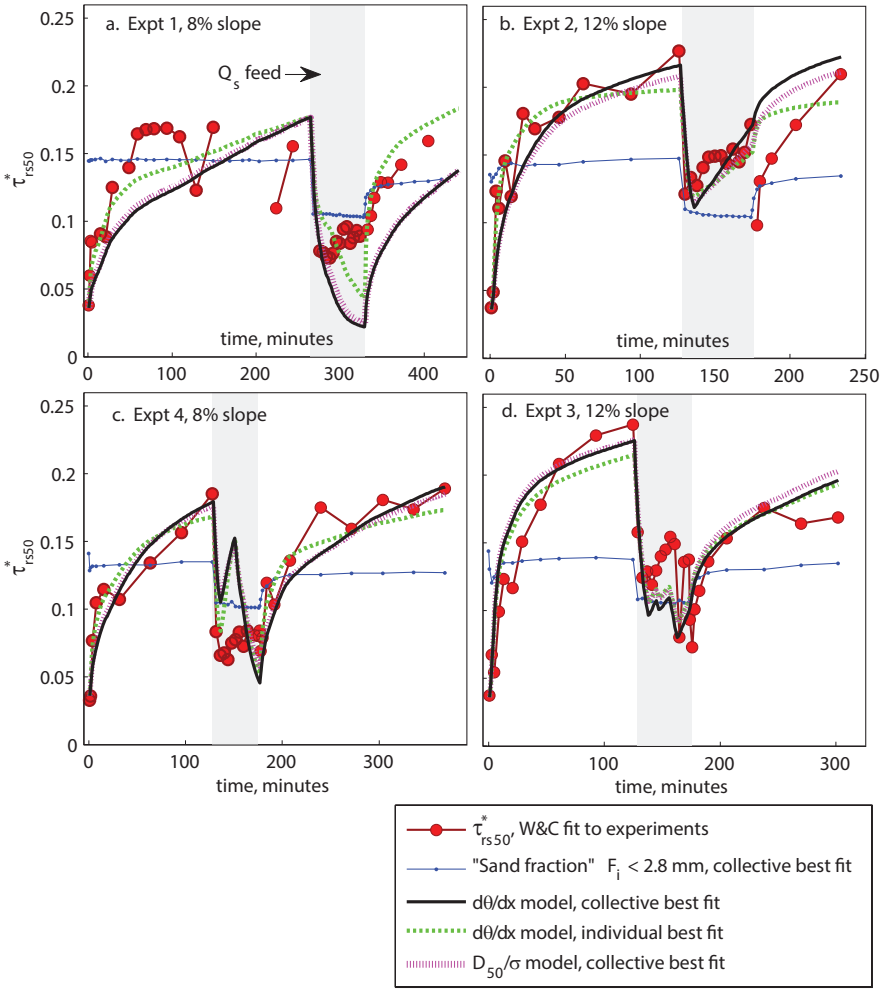

Figure 5. Best-fit models (Eq. 7 and 14) compared to experimental constraints. The periods of upstream sediment supply (Q_{sfeed}) are indicated by the grey boxes for each experiment.

Earth Surf. Dynam. Discuss., doi:10.5194/esurf-2015-52, 2016
Manuscript under review for journal Earth Surf. Dynam.
Published: 19 January 2016

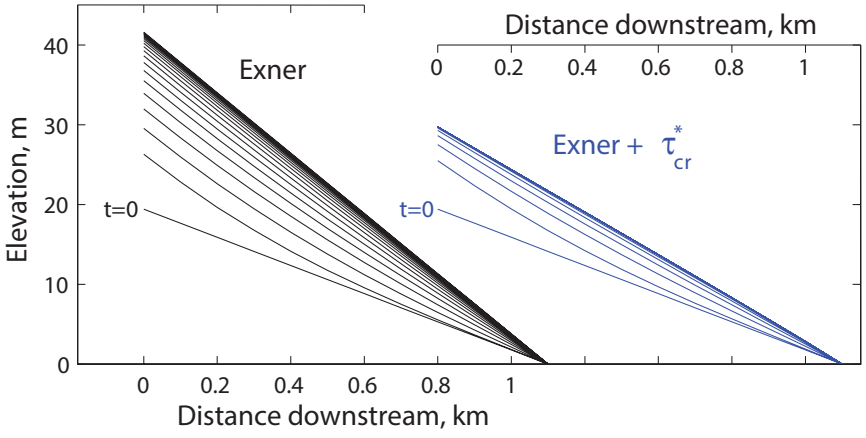

Figure 6. Profile evolution, comparing the morphodynamic responses of models with and without threshold evolution. The initial condition is an equilibrium channel with τ_c^*=0.06, upstream sediment supply q_s=1e-3 m^2/s, and an initial equilibrium slope of 0.0147. Sediment supply is increased 5x at t=0. Lines are each 5 model days apart, and indicate the evolution to a new transport equilibrium.

Earth Surf. Dynam. Discuss., doi:10.5194/esurf-2015-52, 2016
Manuscript under review for journal Earth Surf. Dynam.
Published: 19 January 2016

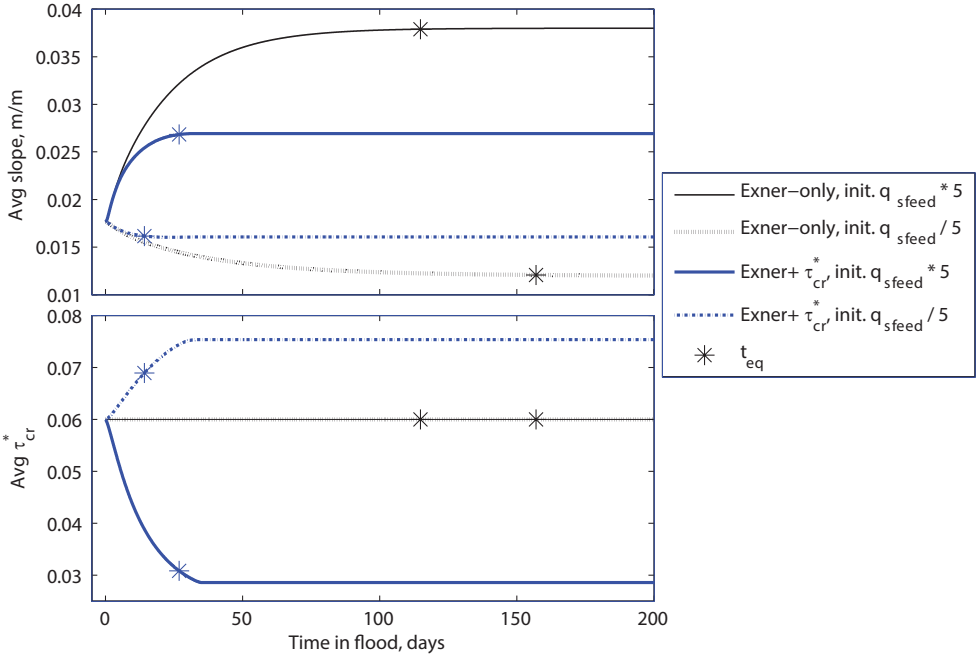

Figure 7. Slope and critical shear stress evolution, for sediment supply increases (which correspond to Fig. 6 models) and decreases by factors of 5. As in figure 6, t=0 corresponds to an equilibrium condition where the initial slope and initial threshold are consistent with the initial upstream sediment supply. Slope and τ_c^* were averaged over model nodes 3-10, leaving out the first and last two nodes because of minor model boundary effects.

Earth Surf. Dynam. Discuss., doi:10.5194/esurf-2015-52, 2016
Manuscript under review for journal Earth Surf. Dynam.
Published: 19 January 2016

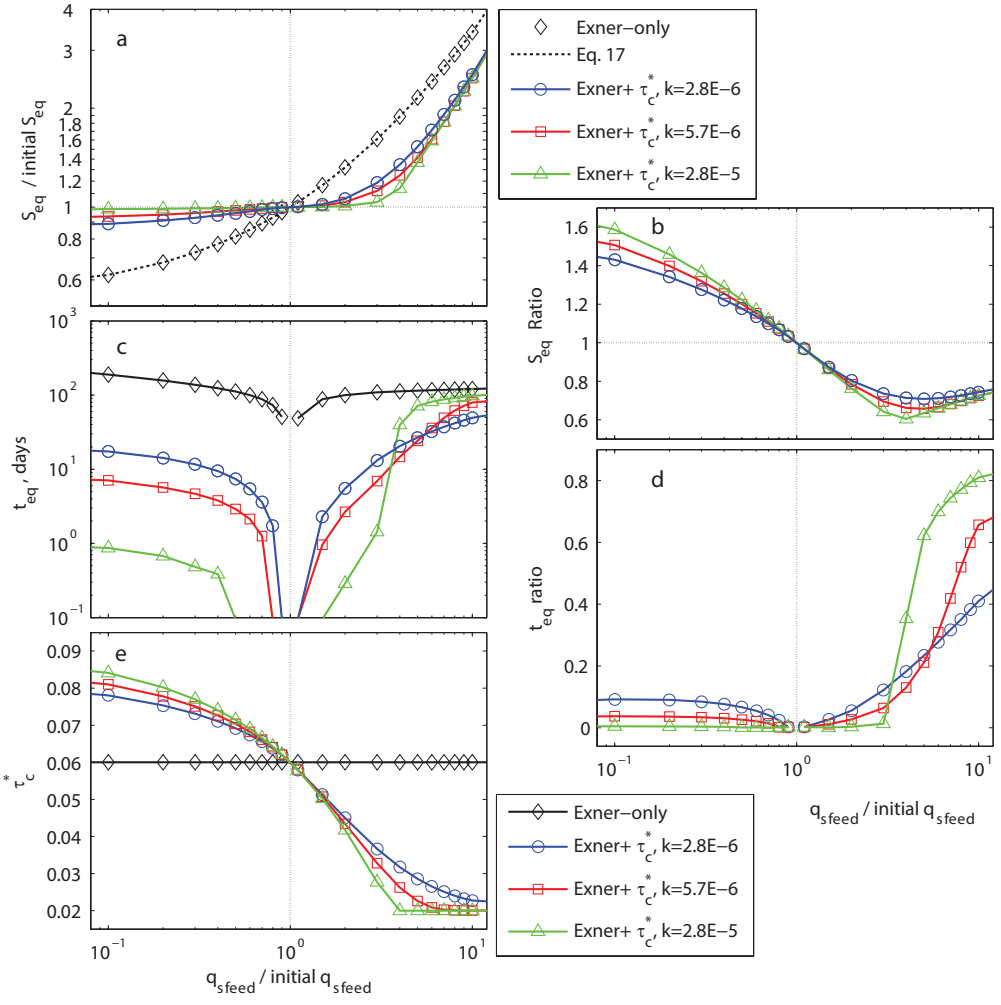

Figure 8. Morphodynamic model sensitivity to sediment supply perturbations and k. All models started at the same equilibrium condition as shown in Fig. 6 and 7. a. Slope adjustment, normalized by the initial equilibrium slope. The correspondence of Eq. 17 and the morphodynamic model calculations demonstrate that the models did asymptotically attain equilibrium slopes. b. S_{eq} ratio is the ratio of equilibrium slopes of the Exner+τ_c^* model divided by S_{eq} for the Exner-only model, to show the relative affect that that τ_c^* evolution has on equilibrium slopes. c. Equilibrium timescales for model adjustment. d. t_{eq} ratio is the ratio of t_{eq} for the Exner+τ_c^* model divided by t_{eq} for the Exner-only model. Values are lower than 1, indicating that the τ_c^* evolution has a large influence on equilibrium timescales. e. Evolution of τ_c^*.

Earth Surf. Dynam. Discuss., doi:10.5194/esurf-2015-52, 2016
Manuscript under review for journal Earth Surf. Dynam.
Published: 19 January 2016

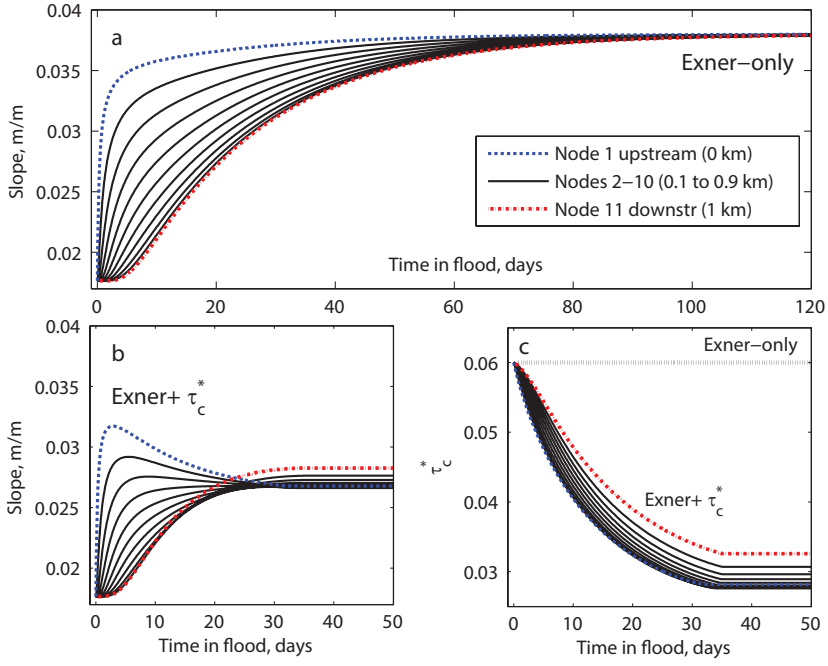

Figure 9. Spatial and temporal evolution of morphodynamic slopes, for the same models shown in Fig. 6. Slope is initially at equilibrium and responds to the 5x increase in upstream sediment supply at t=0. a. The Exner-only model initially has spatial slope variability, but evolves to a uniform new equilibrium slope. b, c. In the model with evolving τ_c^*, slope and τ_c^* variability persist even at equilibrium.

Earth Surf. Dynam. Discuss., doi:10.5194/esurf-2015-52, 2016
Manuscript under review for journal Earth Surf. Dynam.
Published: 19 January 2016

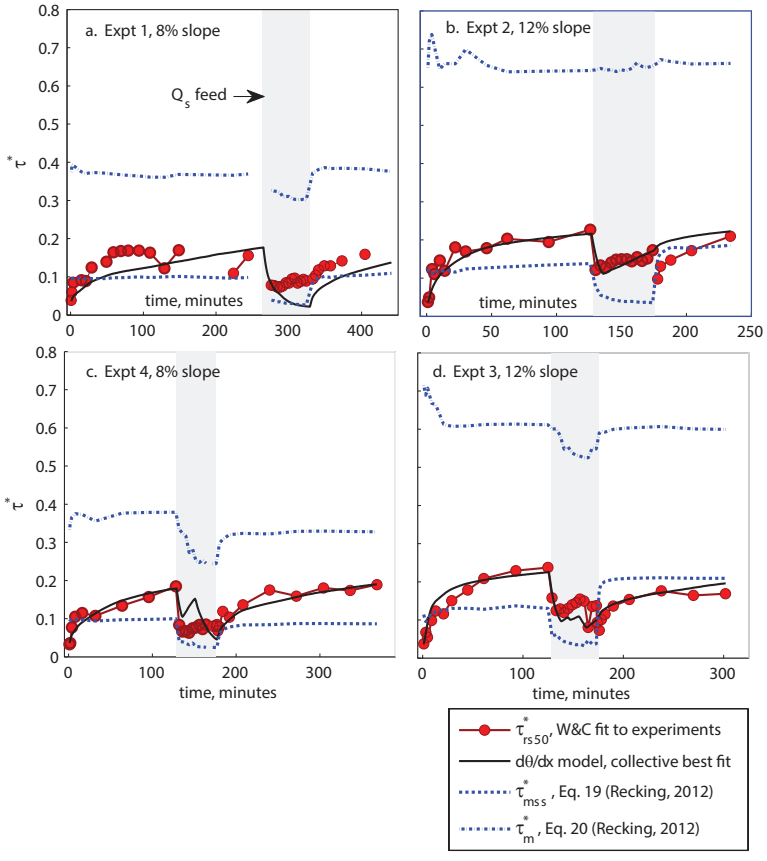

Figure 10. Comparison of experimental and best-fit model constraints on τ^*_{rs50}, compared to proposed constraints for D_{84} reference stress bounds for low and high sediment supply from Recking (2012).

Earth Surf. Dynam. Discuss., doi:10.5194/esurf-2015-52, 2016
Manuscript under review for journal Earth Surf. Dynam.
Published: 19 January 2016

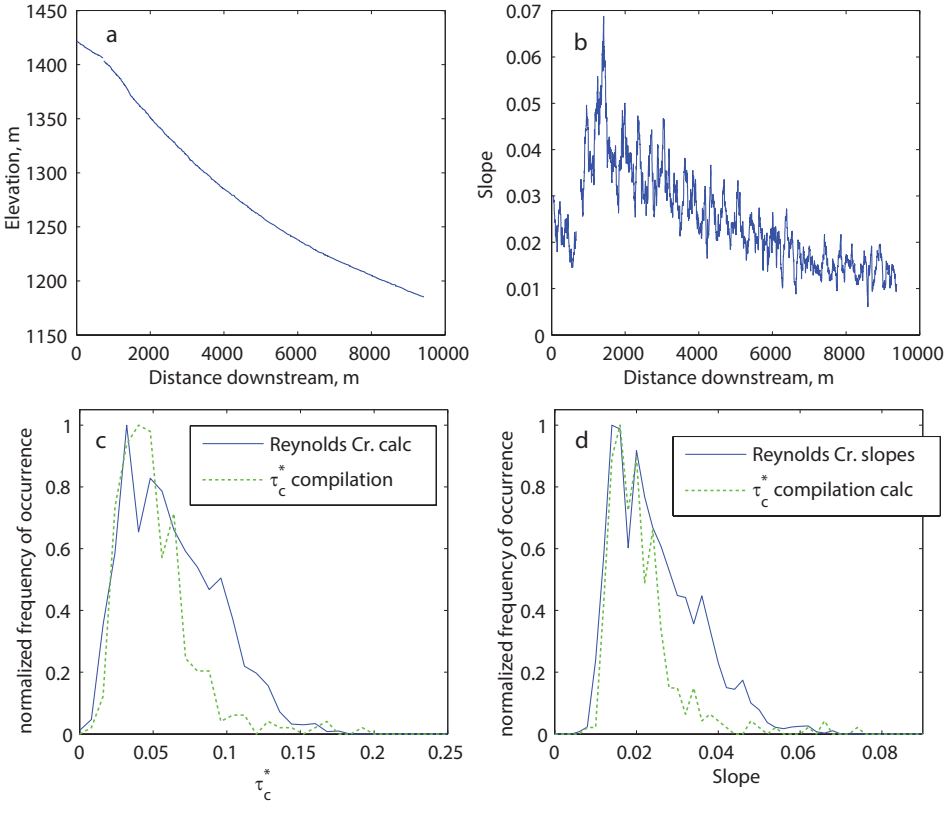

Figure 11. Comparison of Reynolds creek and τ_c^* data compilation predictions using Eq. (18) and (21). a. Longitudinal profile based on airborne Lidar (Olinde, 2015). Upstream end (distance=0) is an arbitrary location along the channel (a bridge). Data gap at 730 m is a gauging station weir; the slope steepens downstream of the weir where the valley becomes constricted by bedrock, although the bed remains almost entirely alluvial. b. Slopes averaged over 100 m reaches, illustrating reach-scale slope variability. c. Histogram of τ_c^* compilation (data shown in Fig. 1), compared to τ_c^* calculated using Eq. (21), based on Reynolds Creek 100 m slopes (panel b), and assuming qw=1 m2/s, q_s^*=2e-3, and f=0.1. d. Similar calculation as panel c, but using Eq. 18 to solve for slope as a function of τ_c^* from the Fig. 1 data compilation, and compared to panel b slopes.